ELSEVIER

Journal of Marine Systems 33–34 (2002) 497–521

JOURNAL OF MARINE SYSTEMS

www.elsevier.com/locate/jmarsys

Coupled Mediterranean ecomodel of the phosphorus and nitrogen cycles

G. Crispi*, A. Crise, C. Solidoro

Istituto Nazionale di Oceanografia e di Geofisica Sperimentale, Borgo Grotta Gigante 42/c, 34010 Trieste, Italy

Received 2 October 2000; accepted 30 July 2001

Abstract

Assessment of the Mediterranean marine environment, in terms of nutrient depletion and easterly decreasing trophic gradients, requires full exploit of the knowledge and processes of the ecosystem dynamics. The three-dimensional model here proposed takes into account the phosphorus and nitrogen cycles coupled with the temporal and spatial hydrodynamical evolution. The food web considers, as primary producers, small autotrophs and large autotrophs uptaking on a multi-nutrient environment characterized by differential remineralizations of the detrital matter components. Grazing effects are modulated by herbivorous zooplankton response. The model is compared with the OCEAN-calibrated chlorophyll averages of the 1979–1985 Coastal Zone Color Scanner (CZCS) satellite data. This procedure validates the model biomass in the Western Mediterranean, which is 0.24 mg Chl m^{-3} when averaged yearly, with CZCS excess of about 10%, and in the Eastern Mediterranean, where the mean is 0.09 mg Chl m^{-3}, with CZCS excess of 25%. The time series of the modelled results are well correlated with the CZCS estimates, with a higher value in the western than in the eastern basin. The temporal and spatial evolution of the biochemical patterns are studied. The effects of the implemented design on phosphorus and nitrogen cycles throughout the food chain are quantitatively followed and compared with results coming from specific cruises. Results about the vertically integrated biomasses are reported, giving an average of 2.7 g C m^{-2} for the total phytoplankton in the western basin and of 1.6 g C m^{-2} in the eastern one. The zooplanktonic biomass attains a mean value of 1.0 g C m^{-2} in the western basin and of 0.3 g C m^{-2} in the eastern one. Average productions accord with plankton abundances, with western primary and secondary productions, respectively, two and three times higher than the eastern ones.

Keywords: Phosphorus; Nitrogen; Food web; Phytoplankton; Mediterranean Sea

1. Introduction

Descriptions in terms of overall biochemistry give the following peculiarities in the Mediterranean Sea.

1. nutrient depletion with respect to the world ocean (Levitus et al., 1993; Denis-Karafistan et al., 1998);
2. oligotrophy of the euphotic zone determining low values of phytoplankton biomass and primary production (Lefevre et al., 1997), except for coastal areas, due to the influence of major rivers, and in some open sea regions, because of permanent gyres and upwellings;

* Corresponding author. Osservatorio Geofisico Sperimentale, P.O. Box 2011, 34016 Trieste, Italy. Tel.: +39-40-2140205; fax: +39-40-327307.

E-mail address: gcrispi@ogs.trieste.it (G. Crispi).

0924-7963/02/$ - see front matter
PII: S0924-7963(02)00073-8

3. significant decadal trends of the nutrients (Béthoux et al., 1992).

Nutrient depletion is a direct consequence of the thermohaline processes taking place in the Mediterranean. The inverse estuarine circulation of the whole basin determines a negative budget for the nutrients at the Gibraltar Strait (Coste et al., 1988), importing nutrient poor surface water from the Atlantic Ocean and exporting relatively nutrient-rich intermediate water.

Oligotrophy is related to the interaction of the general circulation pattern with the productivity inside the basin and with the export production and remineralization along the water column. Permanent and recurrent gyres, mainly cyclones in the northern area of the basin and anticyclones in the southern one, give rise to regional variabilities affecting the vertical import of nutrients, which is the determining factor for new production (Dugdale and Wilkerson, 1988). The influence of these variabilities also on primary production was experimentally assessed in the Western (Berland et al., 1973) as well as in the Eastern Mediterranean (Berman et al., 1984).

To capture the medium- and long-term evolution of the trends involves the main biogeochemical features and, therefore, relies on the knowledge of the general dynamics of the ecosystem (Margalef, 1985). This evidence leads to a conceptual design of the functioning of the Mediterranean ecosystem where both physical, chemical and biological components are important.

There are some recent works for the Mediterranean area on the subject. Marcer et al. (1991) made a 3D analysis of the behaviour of the marine environment; their study was applied to a real bay and fully exploits the nitrogen–phytoplankton–zooplankton food chain determining the sedimentation of biogenic particles. Pinazo et al. (1996) gave the variability of the nitrogen–phytoplankton–detritus food chain on the northwestern Mediterranean shelf using a 3D hydrodynamical model; the grazing loss is simulated here by linear loss in terms of phytoplankton.

The 3D domain reached a subbasin application taking full advantage of a primitive equation model giving realistic fluxes at interfaces in the work by Civitarese et al. (1996); regeneration processes were taken fully into account in the nitrogen–phytoplankton–detritus ecosystem description. Another regional application in the Gulf of Lions was set up by Tusseau-Vuillemin et al. (1998); their model gave the size fractionation growing on nitrate, ammonium and silica of the diatoms and flagellates, while herbivores and protozoa act as external grazing loss for the ecosystem.

A 3D study was proposed using nitrogen–phytoplankton–detritus parameterized for the nitrogen cycle on an overall Mediterranean scale; this model gave chemical fluxes at the principal straits, and seasonal variability of inorganic nitrogen and of phytoplankton (Crise et al., 1998; Crispi et al., 1999).

The study of the onset of the spring bloom in northwestern Mediterranean was carried out by means of nutrient–phytoplankton–zooplankton–detritus model coupled with a primitive equation model (Levy et al., 1999). Also, in Adriatic Sea, a 3D multi-nutient approach has been proposed (Zavatarelli et al., 2000).

The objective of the present work is to integrate the time and space evolution of the Mediterranean lower trophic levels in a three-dimensional model, heretoafter referred to as ECHYM, acronym of "ECoHYdrodynamical model of the Mediterranean." The aims of this model are: (a) to study the phytoplanktonic biomass and its variability, (b) to understand the role of the phosphorus and nitrogen cycles in the ecological processes of the euphotic and intermediate levels, and (c) to obtain the large scale ecological response of the ecosystem to seasonal forcing.

To this purpose, the biological processes are described by an aggregated scheme, that designs the trophic web of nutrients–autotrophs–herbivores chain and the remineralization processes. These trophic levels are regulated by nonlinear diffusion–advection–reaction equations solved at the same grid as the hydrodynamics.

In the next section, the conceptual description of biochemical processes as assessed in the 10 variable ECHYM is briefly given. The mathematical apparatus is fully developed in Appendix A as regards the biological equations.

In the physical forcing section, the coupling of the ecological model with the ecosystem dynamics is explained.

The Parameterization section describes the trimming procedure chosen for the overall Mediterranean integration.

In the Results section, concentrations are analyzed for the biological compartments by average, and surface chlorophyll data are used for validating the model's results; the coupling is discussed taking into account some transects in a specific area; and the phytoplankton behaviour at basin scale is reported, giving an insight into higher trophic levels and productions.

The conclusions summarize the results.

2. Conceptual scheme of the phosphorus and nitrogen cycles

The description of the food web used, the nutrient-driven trophic cycles and their interactions with the microbial loop are shown in Fig. 1. Two different size-fractionated primary producers are considered, the first representing the small autotrophs, the ultraplankton, with size smaller than 10 μm, and the second the large autotrophs, the netplankton, with size larger than 10 μm. Both primary producers compartments grow, each at its own specific rate, depending on the temperature, irradiance level and nutrient availability. As a closure for the food web, the grazing pressure upon primary producers is simulated by a single zooplanktonic compartment. The potentially limiting nutrients used in the model are inorganic nitrogen, both in oxidized and reduced form, and reactive phosphorus. Detrital matter remineralization and fate is dynamically simulated, keeping its phosphorous, nitrogenous and carbonaceous components. The oxygen variable, not included in this diagram, is a prognostic variable whose evolutionary and boundary conditions are described in Appendix A.

The phytoplankton growth limitations are described by Monod kinetic for the uptake of phosphorus, nitrates and ammonia and by Steele formulation for light, whereas the effect of the temperature is simulated by the Lassiter and Kearns (1974) function, whereby the growth rate increases exponentially up to an optimal temperature, and declines above it, and vanishes at the temperature of arrest.

The choice of considering in ECHYM both phosphorus and nitrogen is supported by ongoing research (Thingstad and Rassoulzadegan, 1995). The impor-

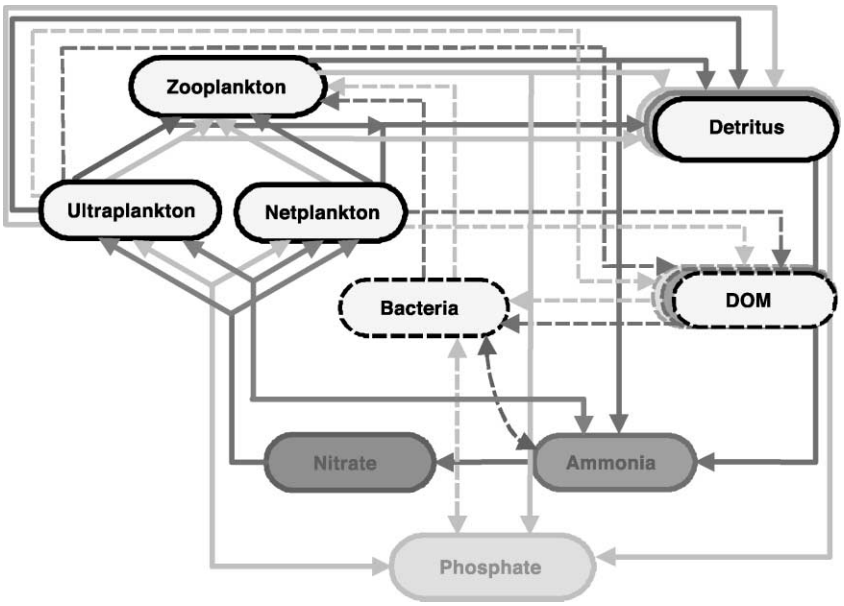

Fig. 1. The biochemical compartments of ECHYM are shown. The arrows represent fluxes flowing from one compartment box into another one; phosphorus fluxes are in light grey, nitrogen ones in dark grey. Ultraplankton, Netplankton and Zooplankton compartments have fixed P:N:C ratios, while Detritus changes its composition accordingly to the overall dynamics. Also, the labile dissolved organic matter, DOM, pools and the free living Bacteria compartment are introduced in this scheme using dashed arrows. These processes are described, as discussed in the text, by first-order kinetics.

tance of phosphorus limitation is due to the skewness of N:P ratio in the Mediterranean Sea, generally above Redfield et al. (1963) oceanic one. The nitrogen role in limiting the phytoplankton growth must be retained for studying areas under the influence of the Mediterranean Atlantic Water and with strong seasonal vertical apport of nutrients, where phosphorus content is relatively higher.

Silicates are not taken into account in the model as contributing to the limiting nutrient factor because they are generally abundant in the euphotic layer (Krom et al., 1993).

The grazing activity is described by a type II functional response (Holling, 1965), modified as in Fasham et al. (1990), to include the possibility of herbivores grazing upon both groups of primary producers. A similar approach was used to simulate primary production with a one-dimensional model in an oceanic environment, using a first-order loss term for small autotrophs and a rectangular shaped hyperbolic grazing for large autotrophs (Bisset et al., 1994). The zooplankton processes, predation, egestion, ingestion, internal matter ratio, excretion and mortality are simulated in line with known phenomenology as reported in the Parameterization section.

The detritus chain describes the recycling of carbon and macronutrients through remineralization of the nonliving organic matter, produced by exogenous input, mortality processes, excretion and exudation, all set as linear processes. The introduction of the detritus compartment permits to follow the particulate matter motion at a basin and subbasin scale, outside the euphotic zone, which is a condition to keep the new production balanced (Eppley and Peterson, 1979).

The flow analysis by Michaels and Silver (1988) shows that, even in oligotrophic environments where picoplankton dominates primary production, netplankton is the main responsible for the sinking of particulate matter. Their approach, based on the Azam et al. (1983) microbial food web, gives this result because of the immediate pressure on netplankton of the flux producer trophic level, namely the herbivorous zooplankton, while there are at least two steps from the nanoplankton and at least three from the bacteria and picoplankton. In ECHYM, the number of trophic steps from the phytoplanktonic groups to the zooplankton is reduced to only one and, thus, the particle production ultimately relies on the calibration of the overall cycles.

In the present parameterization, this shift towards the netplankton production path is resolved using a relatively high value of the ultraplankton exudation rate and an efficiency in the grazing of the netplankton which introduces a temporal delay in the releasing of the matter with respect to the ultraplankton particles remineralization.

The bacteria compartment and the dissolved organic matter fluxes are also to be considered and are introduced in Fig. 1 using dashed boxes and arrows in the scheme. In fact, the relative fluxes are synthesized in the model by first-order kinetics as explained above. Moreover, the fluxes from dissolved organic phosphorus and nitrogen to nutrients, via bacteria, are shunted by the exudation of phytoplankton groups directly into nutrients. Grazing from bacteria is also taken into account by the specific parameterization of the grazing, through the efficiencies, and of the excretion rate of the zooplankton. This procedure is in the same line of reasoning of that used by Steele (1998) in incorporating the microbial loop in a simple nutrient–phytoplankton–zooplankton designed for the oligotrophic Sargasso Sea.

3. Physical submodel

The model spans the Mediterranean basin, with a horizontal spatial discretization of one-fourth degree (182×57 grid points) and with a vertical resolution of 31 levels. The equations describing the nitrogen and phosphorus uptake as well as the grazing and remineralization processes are integrated on the same grid. For a generic biological tracer, BT, the equation is:

$$\frac{\partial \mathrm{BT}}{\partial t} = \mathrm{grid}_{\mathrm{BT}} - (\vec{u}\cdot\nabla)\mathrm{BT} - K_{\mathrm{H}}^{\mathrm{BT}}\nabla_{\mathrm{H}}^{4}\mathrm{BT} + K_{\mathrm{V}}^{\mathrm{BT}}\frac{\partial^{2}\mathrm{BT}}{\partial z^{2}} - w_{\mathrm{BT}}\frac{\partial \mathrm{BT}}{\partial z}.$$

The first term, $\mathrm{grid}_{\mathrm{BT}}$, represents all the sources and sinks for the variable BT. They are determined by the reaction of BT with all the related chemical and biological tracers at a specific point. These terms with their different dependencies are treated in Appendix A.

The second term represents the advection scheme forced by the hydrodynamical equations given beneath. The third and fourth terms give the biharmonic hori-

zontal and the harmonic vertical turbulent diffusivities, respectively, while the last term represents the sinking effects a biological compartment may experience.

The hydrodynamics is based on the following fully 3D primitive equations in a spherical coordinate system (λ, ϕ, z) using the following assumptions: the Boussinesq, the hydrostatic and the rigid-lid approximations:

$$\frac{\partial \vec{v}}{\partial t} + (\vec{u}\cdot\nabla)\vec{v} + \vec{f}\times\vec{v} = -\frac{1}{\varrho 0}\nabla_{\mathrm{H}} p - A_{\mathrm{H}}\nabla_{\mathrm{H}}^4\vec{v} + A_V\frac{\partial^2\vec{v}}{\partial z^2}$$

$$\frac{\partial p}{\partial z} = -\varrho g$$

$$\nabla\cdot\vec{u} = 0$$

$$\frac{\partial T}{\partial t} + (\vec{u}\cdot\nabla)T = -K_{\mathrm{H}}^T\nabla_{\mathrm{H}}^4 T + K_V^T\frac{\partial^2 T}{\partial z^2}$$

$$\frac{\partial S}{\partial t} + (\vec{u}\cdot\nabla)S = -K_{\mathrm{H}}^S\nabla_{\mathrm{H}}^4 S + K_V^S\frac{\partial^2 S}{\partial z^2}$$

$$\varrho = \varrho(T,S,p)$$

The horizontal and vertical components of the velocity $\vec{u}$ are in the preceding equations $\vec{v} = (v_\lambda, v_\varphi)$ and $w = v_z$, respectively; T and S are the temperature and salinity, while p and ϱ represent the pressure and density. The Coriolis parameter is given by $\vec{f} = 2\Omega\sin\varphi\,\vec{k}$ and g is the gravity constant. $A_{\mathrm{H}} = 0.4\times10^{19}$ cm^4 s^{-1} and $A_{\mathrm{V}} = 1.5$ cm^2 s^{-1} are the horizontal and vertical constant eddy viscosity coefficients, while $K_{\mathrm{H}}{}^{\mathrm{T}} = K_{\mathrm{H}}{}^{\mathrm{S}} = 0.4\times10^{19}$ cm^4 s^{-1} and $K_{\mathrm{V}}{}^{\mathrm{T}} = K_{\mathrm{V}}{}^{\mathrm{S}} = 0.3$ cm^2 s^{-1} are the horizontal and vertical constant turbulent diffusion coefficients.

Due to the instability of the water column, the processes are simulated using a procedure that mixes the contents of two adjacent levels, when the column is in an unstable condition, for up to five subsequent iterations. Whenever instabilities of the biochemistry are introduced, all biological sources and sinks are set to zero and the calculation proceeds.

The overall model is driven by interactive heat fluxes (Castellari et al., 1998), climatological forcings through NMC monthly mean winds and using meridionally variant surface irradiance COADS monthly cloud coverage.

In Fig. 2, the initializations are shown for nitrates. For the other variables, the initial fields are chosen as follows: phosphate values are one sixteenth of the nitrate values at each grid point; oxygen is set equal to 250 μM O l^{-1}; netplankton and ultraplankton are both at the 0.1 μM C l^{-1} level; zooplankton is set at 0.01 μM C l^{-1}; all detritus compartments as well as ammonia have null initial values. In this work, no boundary conditions are imposed for geochemistry. In fact, the influence of the main rivers is important, mainly along the shelf, so it can be disregarded on average when analyzing the open sea response. Works by Tusseau-Vuillemin et al. (1998) and by Civitarese et al. (1998) estimate chemical budgets supporting this approximation for Rhone and Po rivers, respectively.

4. Parameterization

All the parameters of the ecosystem are collected in Table 1. Brief comments about the ecological implications are given in this section.

Both size-fractionated phytoplanktonic groups grow with the same limitation in light, but with slightly different limitations in temperature, with a greater optimal value for the ultraplankton. They uptake with different growth rate parameters; higher for netplankton (Brand and Guillard, 1981) than for ultraplankton (Kana and Glibert, 1987). The half-saturations are those typical of oligotrophic environments, generally favourable to smaller cells. The inhibition coefficient for the nitrate uptake in presence of ammonia is the same for both phytoplankters and is set to the value given in Wrobleski (1977). The respiration, exudation and lysis parameters for netplankton are close to steady-state outcomes (Sakshaug et al., 1989). The ultraplankton group gets loss terms consistently reduced by an amount proportional to its minor growth rate with respect to netplankton one, giving, moreover, a greater extent to exudation recycling than to lysis, as discussed above. For both groups, the P:N:C internal composition is taken equal to the Redfield et al. (1963) fixed ratio.

The zooplankton grazes on both ultraplankton and netplankton through a rectangular hyperbolic expression, driven by the same grazing rates and half-satu-

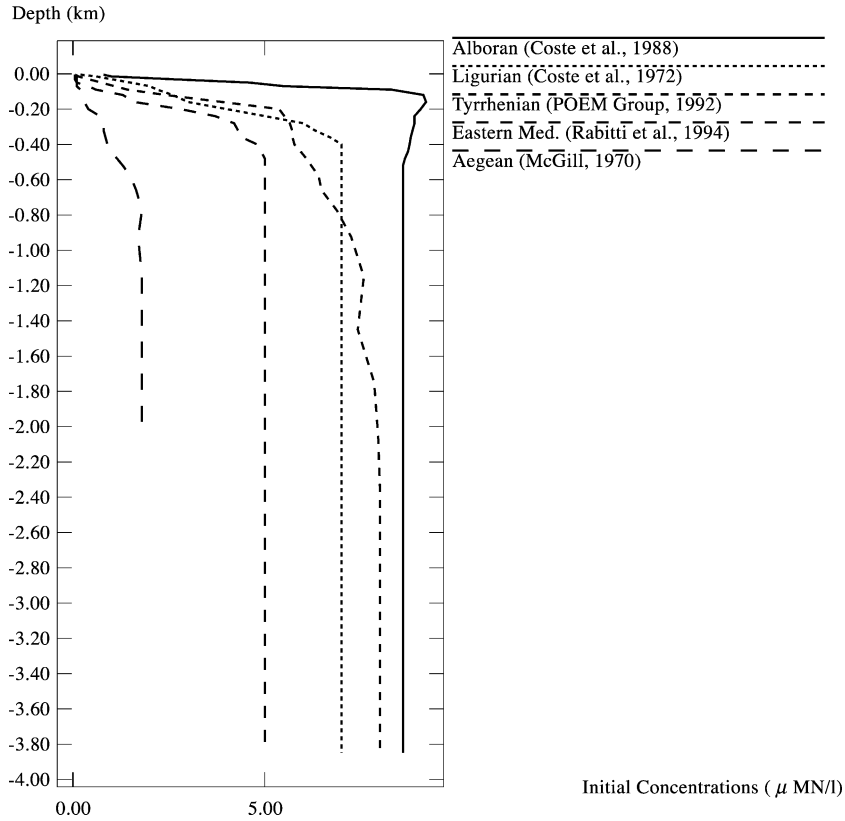

Fig. 2. Nitrate initial profiles, in μM N l^{-1}, in the different areas of the Mediterranean Sea. (Data from Coste et al., 1972, 1988; McGill, 1970; POEM Group, 1992; Rabitti et al., 1994 a,b).

rations, using values typical for herbivores (Fasham et al., 1990). Anyway, the P:N:C for the zooplankton composition is fixed at a different ratio to the Redfield one in line with the stoichiometry of the herbivorous taxonomy (Beers, 1966). The temperature dependence of excretion doubles the value every 10 °C (McLaren, 1965). The specific mortality does not depend on physical parameters and is chosen as a typical temperate area average (Davis, 1987), while the excretion is in agreement with the relation given in Wen and Peters (1994). The efficiency parameters focus the prevalent path from the phytoplanktonic group to zooplankton. In fact, the efficiency from the ultraplankton to the herbivores is smaller than that from the netplankton in line with increasing nitrogen with respect to phosphorous release rates at decreasing daily excretion.

Remineralization and fate of detritus compartments are followed, introducing different remineralization rates: faster for the phosphorous compartment, intermediate for the nitrogenous one, and slower for the carbonaceous one. The average sinking velocity of the detrital compartment is kept as evaluated in a single nutrient model (Crise et al., 1998).

The dynamics of the nitrification processes are analysed as in Zakardjian and Prieur (1994), also in terms of ammonia oxidation. The chlorophyll to carbon ratio in the ultraplankton is chosen as twice that of the netplankton compartment. This is in agreement with field measures by Eppley et al. (1977) and by Glover et al. (1988) and confirmed by laboratory experiments by Llewellyn and Gibb (2000). This doubling from nutrient-rich to nutrient-limited situations is also well represented by a cell-based model description (Zonneveld, 1998).

As the above discussion illustrates, the choice of all parameters is carried out starting from laboratory analyses and from in situ data. The calibration is done following a general line of reasoning about size-frac-

Table 1
List of ecological parameters

Parameter	Definitions	Units	Values
μ_S	maximum growth rate of ultraplankton	s^{-1}	1.60×10^{-5}
k_{PS}	phosphorus half-saturation of ultraplankton	mg at P m^{-3}	0.015
k_{NS}	nitrogen half-saturation of ultraplankton	mg at N m^{-3}	0.15
k_{AS}	ammonia half-saturation of ultraplankton	mg at N m^{-3}	0.15
ψ_S	ammonia inhibition coefficient for ultraplankton	mg at N^{-1} m^{-3}	1.5
μ_L	maximum growth rate of netplankton	s^{-1}	3.20×10^{-5}
k_{PL}	phosphorus half-saturation of netplankton	mg at P m^{-3}	0.025
k_{NL}	nitrogen half-saturation of netplankton	mg at N m^{-3}	0.25
k_{AL}	ammonia half-saturation of netplankton	mg at N m^{-3}	0.25
ψ_L	ammonia inhibition coefficient for netplankton	mg at N^{-1} m^{-3}	1.5
k_{nit}	nitrification rate	s^{-1}	1.11×10^{-5}
k_{AO}	nitrification half-saturation for oxygen	mg at O m^{-3}	31.25
R_{NC}	nitrogen to carbon ratio in phytoplankton	mg at N/mg at C	0.1509
R_{PC}	phosphorus to carbon ratio in phytoplankton	mg at P/mg at C	0.0094
R_{SL}	chlorophyll to carbon transformation quota		2.
r_{NC}	nitrogen to carbon ratio in zooplankton	mg at N/mg at C	0.25
r_{PC}	phosphorus to carbon ratio in zooplankton	mg at P/mg at C	0.0208
R_{OC}	oxygen to carbon ratio	mg at O/mg at C	1.
R_{nit}	nitrification oxygen	mg at O/mg at N	2.
k_{decC}	carbon remineralization rate	s^{-1}	0.59×10^{-6}
k_{decN}	nitrogen remineralization rate	s^{-1}	1.18×10^{-6}
k_{decP}	phosphorus remineralization rate	s^{-1}	2.36×10^{-6}
k_{rS}	ultraplankton respiration rate	s^{-1}	0.068×10^{-6}
k_{rL}	netplankton respiration rate	s^{-1}	0.127×10^{-6}
k_{eS}	ultraplankton exudation rate	s^{-1}	0.289×10^{-6}
k_{eL}	netplankton exudation rate	s^{-1}	0.359×10^{-6}
k_{exz}	zooplankton excretion rate	s^{-1}	0.289×10^{-6}
ϵ_S	ultraplankton efficiency		0.25
ϵ_L	netplankton efficiency		0.50
g	zooplankton grazing rate	s^{-1}	1.157×10^{-5}
α	preference coefficient		1.
k_H	grazing half-saturation	mg at C m^{-3}	4.
d_S	ultraplankton lysis	s^{-1}	0.222×10^{-6}
d_L	netplankton lysis	s^{-1}	0.555×10^{-6}
d_Z	zooplankton mortality	s^{-1}	0.289×10^{-6}
θ	arrhenius base	exp ($°C^{-1}$)	1.07
T_0	arrhenius reference temperature	°C	20.
T_{Smax}	maximum ultraplankton temperature	°C	30.
T_S	ultraplankton optimal temperature	°C	19.5
b_S	ultraplankton temperature coefficient	$°C^{-1}$	0.1157
T_{Lmax}	maximum netplankton temperature	°C	24.
T_L	netplankton optimal temperature	°C	16.5
b_L	netplankton temperature coefficient	°C	0.1157
I_{opt}/I_0	Optimum light ratio		0.5
K_H^{BT}	horizontal turbulent diffusion	cm^4 s^{-1}	0.2×10^{19}
K_V^{BT}	vertical turbulent diffusion	cm^2 s^{-1}	1.5
NCON	mixing iterations		5
w_D	detritus sinking velocity	cm s^{-1}	0.0058
k_{aer}	reaeration surface coefficient	s^{-1}	1.157×10^{-5}

The functional dependences are reported in Appendix A.

tionated counting. In fact, the evidence from polar oceanic areas shows a prevalence of larger individuals, size > 10 μm, when eutrophic conditions are experienced, while a symmetrical reverse is observed in oligotrophic conditions with the dominance of the smaller fraction, size < 10 μm, (Shiomoto et al., 1997; Fiala et al., 1998). In the Mediterranean too, similar assumptions can be made, assigning the prevalence of netplankton to the periods in which mixing is generally important in the months from December to April, while the other months are dominated by the ultraplankton. This partition permits a trimming of the netplankton and ultraplankton specific efficiences in Mediterranean.

5. Results

5.1. Biological seasonal evolution

The biomass concentrations in μM C l^{-1}, as integrated all over the basin along the 5 years of the central simulation, are shown in Fig. 3. The chosen parameterization is able to maintain a quasi-stationary evolution in the period considered. The simulation correctly reproduces the rise of the spring blooms for both phytoplanktonic groups. The model shows a netplankton bloom in the early spring, followed by the ultraplankton one, which reaches it maximum productivity at higher levels of light intensity and temperature. Such blooms cause rapid depletion of nutrients and formation of sinking particles. The grazing activity starts affecting the phytoplanktonic stocks at the end of the spring after both phytoplankton groups are fully developed. A lower late-summer secondary maximum is present only in the ultraplankton evolution.

The ultraplankton in full line has the greatest values, on average 58% of the total phytoplankton, with respect to 42% of the netplankton during the last 3 years of the simulation. Both variables reach a minimum value in early winter, which is very stable along the simulation when, after 2 years, a quasi-stationary cycle is reached, and the same appears also true for the maxima. The total phytoplankton range lies in the interval from minimum 1.6 g C m^{-2} to maximum 3.2 g C m^{-2} when vertically integrated.

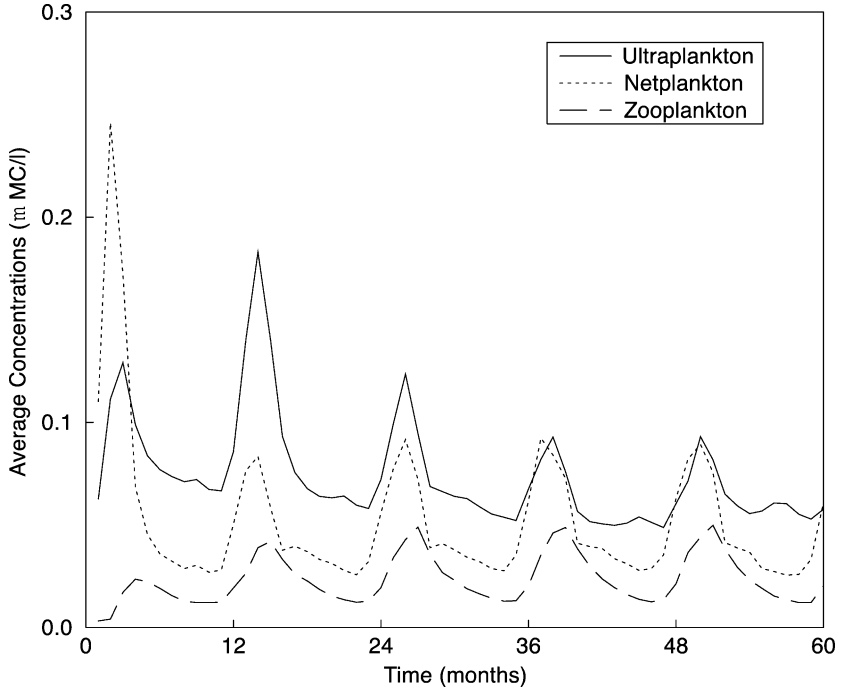

Fig. 3. Time evolution concentrations, in μM C l^{-1}, integrated all over the basin of ultraplankton (full line), of netplankton (dotted line) and of zooplankton (dashed line) for the 5-year model integration.

Thus, the maximum of the phytoplankton biomass is about twice its lower values reached during the summer.

The zooplankton is shown by a dashed line. Its average value is only a fraction of the total phytoplankton and attains 23% always during the last 3 years of the simulation. Average minima are 0.2 g C m^{-2}, while maxima reach 0.9 g C m^{-2}. From these values, zooplankton maximum attains more than four times its minimum, which is reached during late summer.

The buoyancy content, b, of the upper layer of the ocean up to the generic depth, z_0, is by definition the work needed to destroy stratification, i.e. the potential energy calculated starting from z_0 to surface given by:

$$b(z_0) = g \int_0^{z_0} \mathrm{d}z \frac{(\rho(z_0) - \rho(z))}{\rho(z_0)}.$$

The buoyancy content is per se a quantity that is not related to a specific process capable of affecting, in principle, the vertical density distribution in the ocean (turbulent diffusivity, convection, mixed layer dynamics, internal wave breaking, lateral advection, mesocale processes, etc.). Instead, it represents the net effect of all the above processes, thus reproducing, in a quantitative way, what is qualitalively known as the 'mixing-stratification' seasonal cycle of the upper ocean. The higher the buoyancy in a layer, the higher the work to homogenize the water column.

The importance of the buoyancy content for a biogeochemical model stems from the fact that its variability shows how and when the stratification prevents an efficient import of the nutrient pool present below the euphotic layer in the euphotic zone. As shown in Crise et al. (1999), the DCM meridional average in the Mediterranean Sea is deepest in the oligotrophic water of the Levantine basin and shallowest in the Alboran Sea, producing a prominent west–east gradient. Assuming that the nutricline starts at 90 m, on average, in the Western Mediterranean and at 160 m in the Eastern Mediterranean, the average buoyancy content, calculated from the base of the nutricline for each subbasin, is generically defined as:

$$b_{xM} = \frac{1}{xM} \int \int_{xM} \mathrm{d}S b(S)$$

where xM in turn identifies Eastern and Western Mediterranean area and S is the surface.

In Fig. 4a, the evolutions of b in the two basins are superposed, showing a coincident minimum (i.e. the less stratified water column) in correspondence with late winter and a maximum in the late autumn and stronger in the eastern basin due to the higher surface temperature found in the surface layer.

The phytoplankton concentrations for the Western and Eastern Mediterranean, integrated within the base of the nutricline, shown in Fig. 4b, reach a quasi-stationary stage after 2 years. This result stresses the fact that the eastern basin converges to a quasi-stationary stage faster and exhibits similar amplitudes confirming at basin scale what was inferred by Turley et al. (2000) from chlorophyll data. A delay in the onset of the late winter bloom of about 2 months, January for the Western and March for the Eastern Mediterranean, is present, however not related to the density structure of the water mass in the upper layer.

In the two subbasins, a plot of the depth integrated phytoplankton concentration split into netplankton and ultraplankton again shows an evident difference between the autotrophic biomass concentrations of the eastern and western basin, much higher in the western one. Again, on the western side, netplankton dominates in all seasons (Fig. 4c), while on the eastern side, the opposite is true (Fig. 4d). Therefore, the depth of the nutricline and the buoyancy content influence the concentration of the biomass of each subbasin, but they do not affect the total biomass present in the water column within the euphotic zone.

The modelled seasonal averages for the surface chlorophyll are shown in Fig. 5. The model's results average the third, fourth and fifth years of the simulation. This average is maintained in Figs. 7–12 and in Tables 2, 3 and 4. In winter (Fig. 5a), the surface bloom is evident in the modelled chlorophyll, in particular, in the Western Mediterranean with higher values in the northwestern Mediterranean, about 2 mg Chl m^{-3}, and lower values, down to 0.05 mg Chl m^{-3}. This is due to the deep nutrients available in surface layer because of the mixing processes. In spring (Fig. 5b), a clear west–east decreasing difference, about 1 mg Chl m^{-3}, is evident with a maximum in the Alboran Sea and a minimum in the Levantine Sea. In particular, the Alboran Sea peak chlorophyll due to the permanent hydrodynamical structures is evident, as well as the Spanish coast upwelling in the Balearic Sea and in the Ligurian–Provençal basin. The biological effects

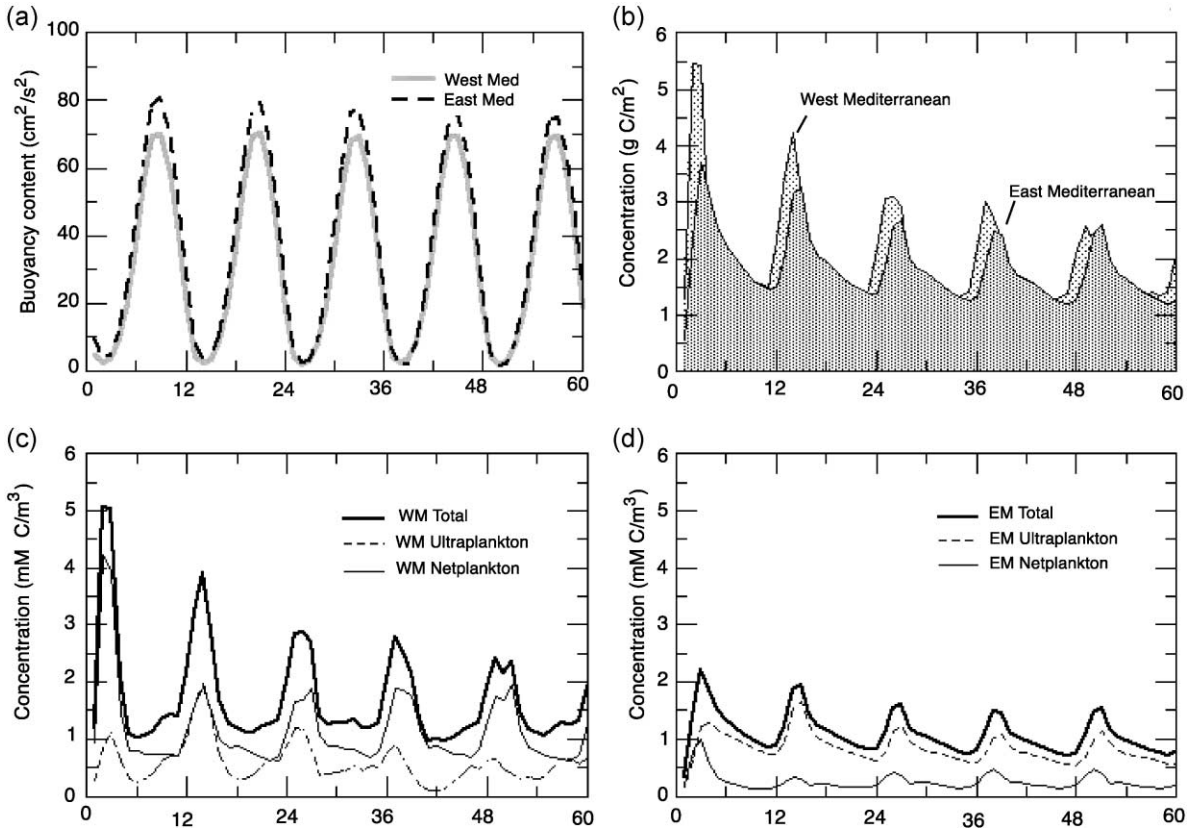

Fig. 4. Evolution in the 5 years of the simulation of (a) average buoyancy content ($cm^2\ s^{-2}$); (b) depth-integrated phytoplankton over the euphotic layer (g C m^{-2}); (c) Western Mediterranean size-fractionated phytoplankton concentrations (mM C m^{-3}); (d) Eastern Mediterranean size-fractionated phytoplankton concentrations (mM C m^{-3}).

caused by upwelling along the south coast of Sardinia, Sicily and the south-east coast of Italy are evident. In summer (Fig. 5c), the depleted situation is reached, with values of the order of 0.05 mg Chl m^{-3} or less. In autumn (Fig. 5d), the modelled surface chlorophyll begins to grow again and follows the circulation patterns, with the minima in the southern regions and in the Levantine basin and the maxima in the Alboran Sea. The coast of Sicily is slightly affected by upwelling. Generally, the patterns are lower in the eastern than in the western part, where there is also greater seasonal variability.

The seasonal variability of the upper layer chlorophyll is available from the Coastal Zone Color Scanner (CZCS) scenes taken by the satellite Nimbus-7, funded by NASA's Mission to Planet Earth Program. Here, the seasonal averages from 1979 to 1985 are considered as analyzed in the OCEAN Project by the EC Joint Research Centre and the European Space Agency (Barale et al., 1999; Sturm et al., 1999). The integer data, *bd*, are transformed into chlorophyll concentrations using the transformation:

$$\mathrm{Chl} = \mathrm{e}^{(bd-128)/36}.$$

The sequence of seasonal averaged images (Fig. 6) show that the maxima are obtained in winter, decreasing in spring. In summer, the pigment concentrations show their lowest values, followed by a new increase in autumn, particularly where upwelling or eddies are present. The patterns are lower in the eastern part than in the western one, where there is also a greater seasonal variability. Here is also evident signature of the most important rivers, Rhone, Po, Ebro, Nile. They

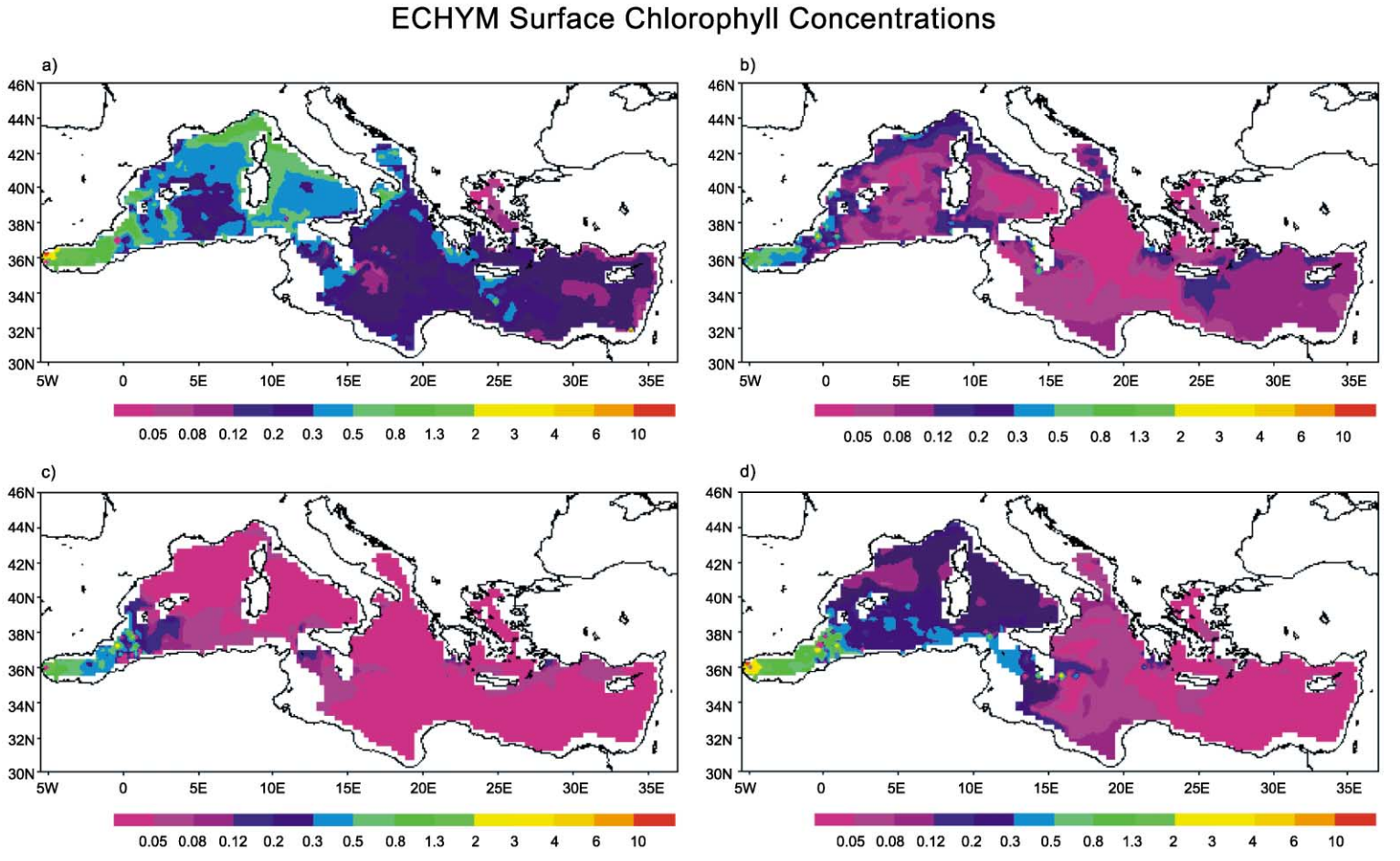

Fig. 5. ECHYM model surface chlorophyll concentrations (mg Chl m^{-3}) in (a) winter, (b) spring, (c) summer and (d) autumn. The areas deeper than 200 m are shown.

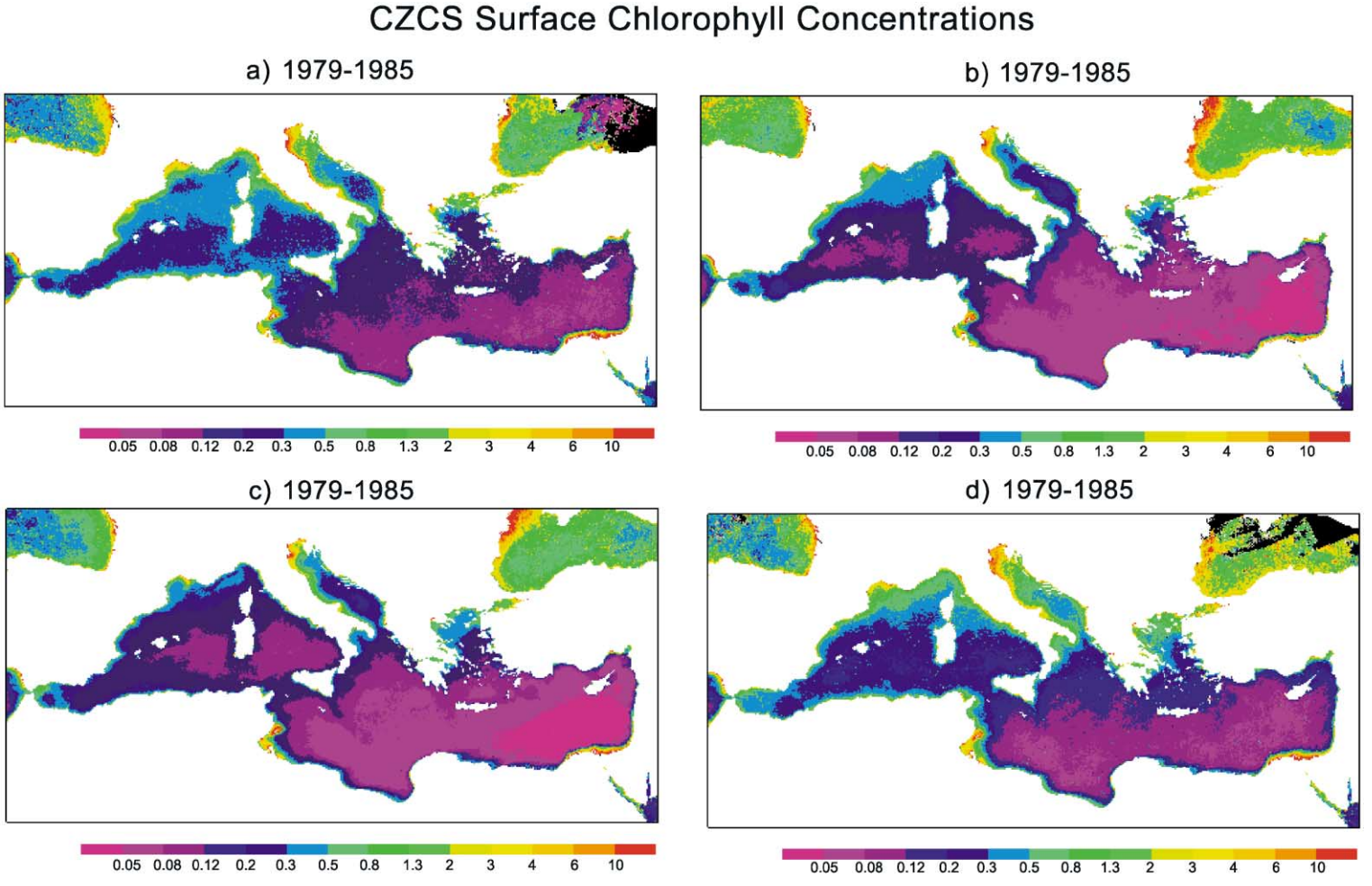

Fig. 6. CZCS surface chlorophyll concentrations (mg Chl m^{-3}) in (a) winter, (b) spring, (c) summer and (d) autumn. The areas in black represent missing data.

give an important contribution to the primary production as well as to the total suspended matter present in their plumes. Anyway, the interaction with the open sea is clearly confined inside the shelf areas adjacent to these rivers.

To give a quantitative description of the distance between the model and data in Fig. 7a, the monthly averages are split in the Western Mediterranean for ECHYM and for CZCS in areas with a depth greater than 200 m. The values are of the same order with an annual mean for the model 0.24 mg Chl m^{-3}, with CZCS value, 0.26 mg Chl m^{-3}, about 10% higher than model's result. The maximum values happen for both curves in January, while minima are reached in the summer months. The variability is greater in the model than in the CZCS. This excursion is expressed by the model's standard deviation, which is about twice as large as the CZCS one. The correlation between the two series is very high with a value of 0.80. This marks a very good resemblance of the model's averaged surface chlorophyll concentrations with respect to the satellite ones.

In Fig. 7b, the model and the CZCS average monthly values are given in the Eastern Mediterranean, where areas deeper than 200 m for both curves are again considered. The averages here are 0.09 mg Chl m^{-3} for the model and 0.12 mg Chl m^{-3} for the CZCS, with 25% in excess of CZCS with respect to the model. In any case, the behaviour is respected with the maximum value in February for both series and very low values in summer. The values are more than twice lower than those attained in the western basin. Also, the variance in the model is about twice the CZCS estimation. Correlation in this case gives a value equal to 0.65, still high but lower than in the western case.

5.2. Nutrient cycles

In Fig. 8, the limitations of the primary producers are shown in function of the temperature and nutrient distributions during April at the surface 20-m layer, when the permanent stratification in the overall Mediterranean begins to appear. The temperature factor for the ultraplankton, upper left plate, and the netplankton, upper right plate, are shown. From this analysis, a comparison between netplankton and ultraplankton on temperature dependency shows that the larger one is favoured in the northwestern Mediterranean, while in the eastern basin, the two fractions have a similar temperature limitation. The total nutrient limitations in the lower plates, multiplied by the specific maximum growth rates, are shown for the ultraplankton, left plate, and for the netplank-

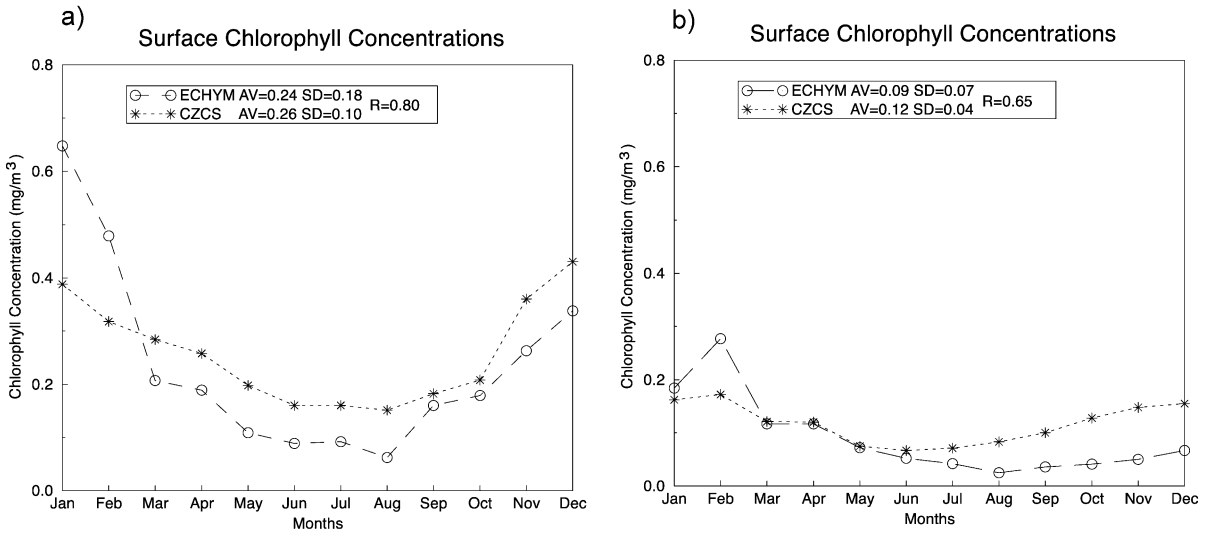

Fig. 7. Surface chlorophyll concentration (mg Chl m^{-3}) monthly averaged in Western Mediterranean (a) and in Eastern Mediterranean (b) in areas deeper than 200 m. Averages, standard deviations and correlation coefficients are also reported.

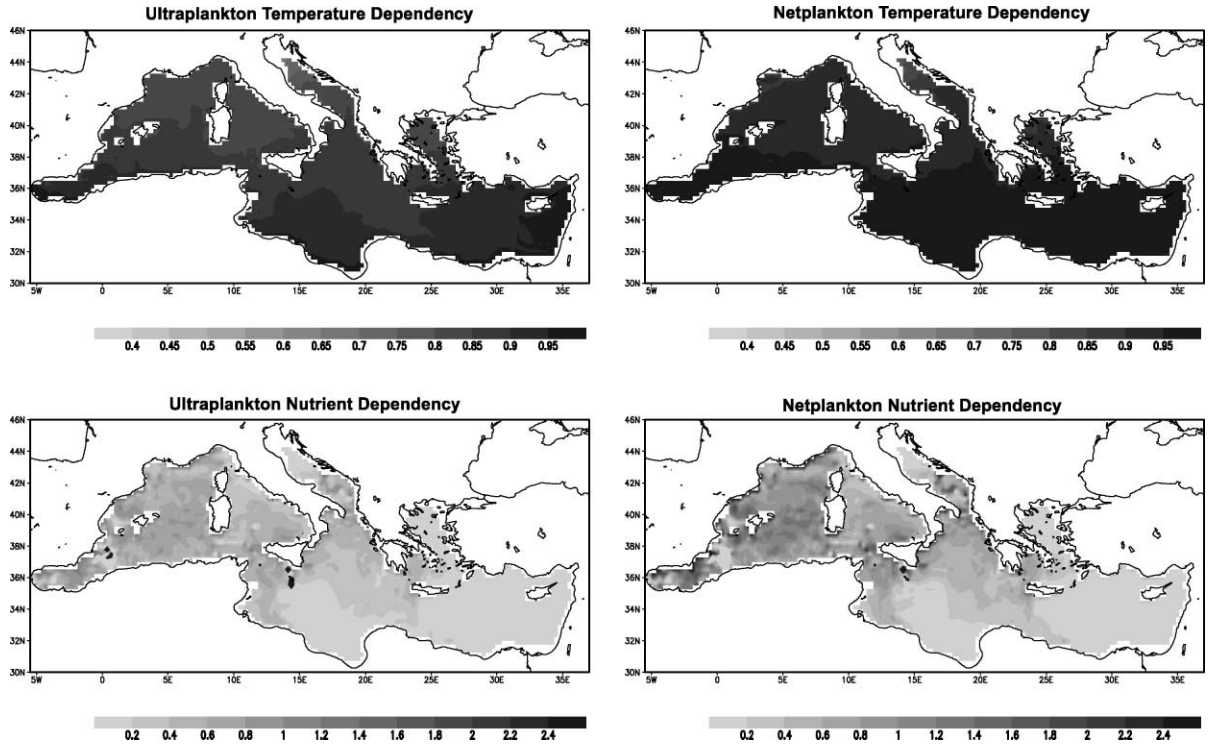

Fig. 8. Temperature (upper plates, dimensionless) and nutrients (lower plates, day^{-1}) limitations of ultraplankton (left) and of netplankton (right) growths at the surface 20-m layer in April.

ton, right plate. The situation is generally favourable to the netplankton in spite of its higher half-saturation parameter due to its higher specific growth rate (1.38 day^{-1} for ultraplankton and 2.76 day^{-1} for netplankton, respectively). In some oligotrophic areas of eastern basin, netplankton and ultraplankton show similar nutrient limitation. Being the total growth rate obtained as a product of the temperature, nutrient and irradiance limitation terms, the overall situation is favourable to netplankton growth.

Fig. 9 is the analogue of Fig. 8 in October, near the end of the stratification period. The limitations are shown at the upper 20-m layer for temperature, upper plates, and for the nutrient lower plates (Fig. 9) also in October. Here, temperature effects are dominant with maxima, i.e. low limitations for ultraplankton everywhere in the western and in the northern areas of the eastern basin. The netplankton is generally penalized except in some northern coastal areas of both basins, while in the southern and eastern parts of the Ionian–Levantine, its growth is inhibited by high temperature. The nutrients' dependence is nearly similar for both, with a slight prevalence of the netplankton in southwestern Mediterranean. This cannot reverse the combined situation, which is highly favourable to the growth of the ultraplankton.

It is worth noting that in the two periods shown, the nutrient limitation, obtained by normalizing nutrient dependency using 1.38 and 2.76 day^{-1}, respectively, is always stronger than temperature one, even in the northwestern area. A notable exception is when in October temperature exceeds the netplankton temperature of arrest.

The onset of late winter bloom, and the variability it induces, is evidenced along a transect in the northwestern Mediterranean at 42.5N 4–8E (Fig. 10). In the upper plates, the temperature (shaded) and the salinity (contoured), for the analysis of the thermohaline conditions, and the nitrate (shaded) and phosphate (contoured), for the chemical situation, are visualized during March in the upper 300 m. Temperature and salinity distributions show clear

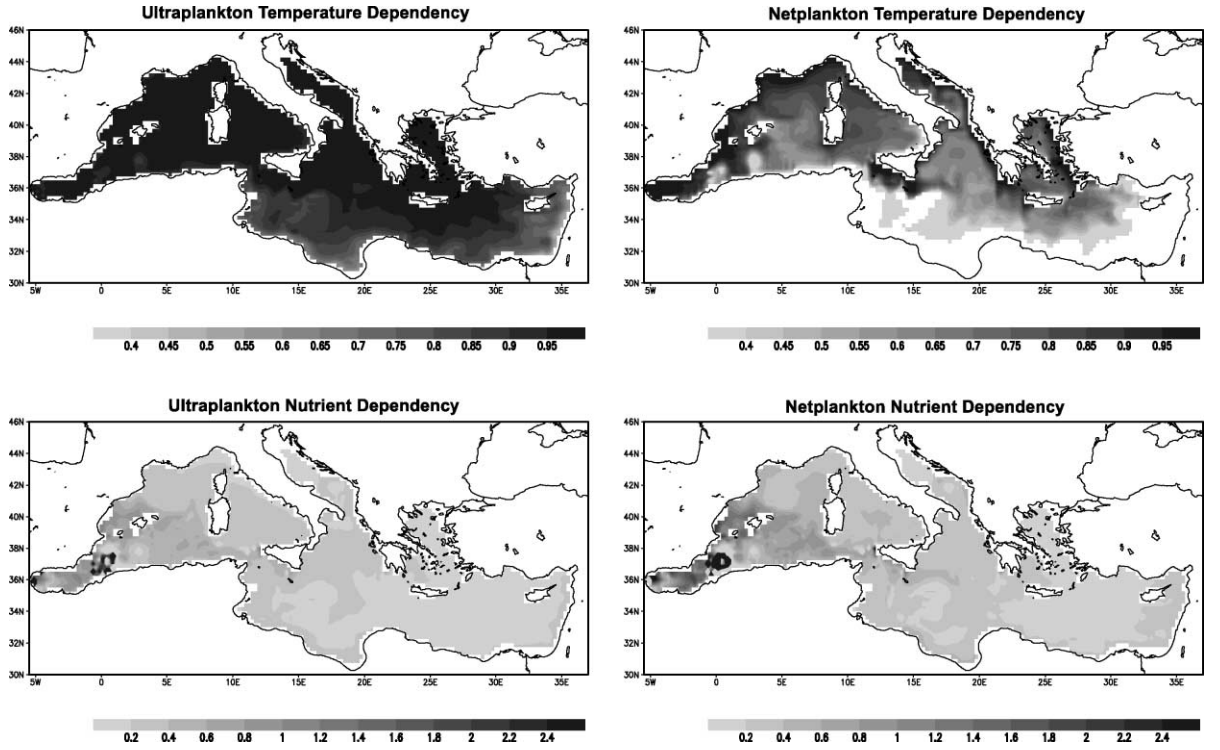

Fig. 9. Temperature (upper plates, dimensionless) and nutrients (lower plates, day^{-1}) limitations of ultraplankton (left) and of netplankton (right) growths at the surface 20-m layer in October. Missing shading represent null values of the temperature limitation.

mixing conditions to 250 m down in the western part of the transect, while the eastern part of the basin shows stratification below a depth of 180 m. Nutrients give a similar situation with the nutricline at 180–200 m, with a mixing in the western area. Phosphate concentrations reach high values, up to 0.18 μM P l^{-1}, while nitrates are about 2 μM N l^{-1} in the surface layer.

The concentrations of the biological variables are given in the lower plates with the ultraplankton (shaded) and netplankton (contoured) and with the total sum (shaded, defined as the sum of ultraplankton and netplankton) and zooplankton (contoured). The high values of the ultraplankton are in the western part of the transect and in one surface area of the transect. This is due to the fact that the downwelling conditions do not import nutrients to the surface layers; thus, these conditions favour the smaller cells. Otherwise, in the eastern part of the transect, there are upwelling conditions, with an increase of nitrate and phosphate along the water column. This trophic regime favours the netplankton bloom. The higher values of the total phytoplankton, from 1 to 2 μM C l^{-1}, cover the area of nutrient minima. Zooplankton is nearly constant, approximately 0.5 μM C l^{-1} in the first 150 m and has an abrupt diminution to one fifth of this value in the following 100 m.

The same transect is shown in April (Fig. 11). The mixing record is still present in the western area, but with a newly formed capping in temperature, which becomes stronger in the eastern part. Nutrients represent a similar situation with mixing in the western area, and the nutricline are clearly present from 30 to 80 m in the eastern and central parts. Strong oligotrophic conditions persist in the first 30 m. Ultraplankton and netplankton distributions show a bloom of netplankton up to 4.5–5.5 μM C l^{-1} in the upper part, the first 60 m; the values are lower for ultraplankton, approximately 1.4 μM C l^{-1}. The latter occupies the central part, while the former is ubiquitous prevaling in the eastern part. The zooplankton

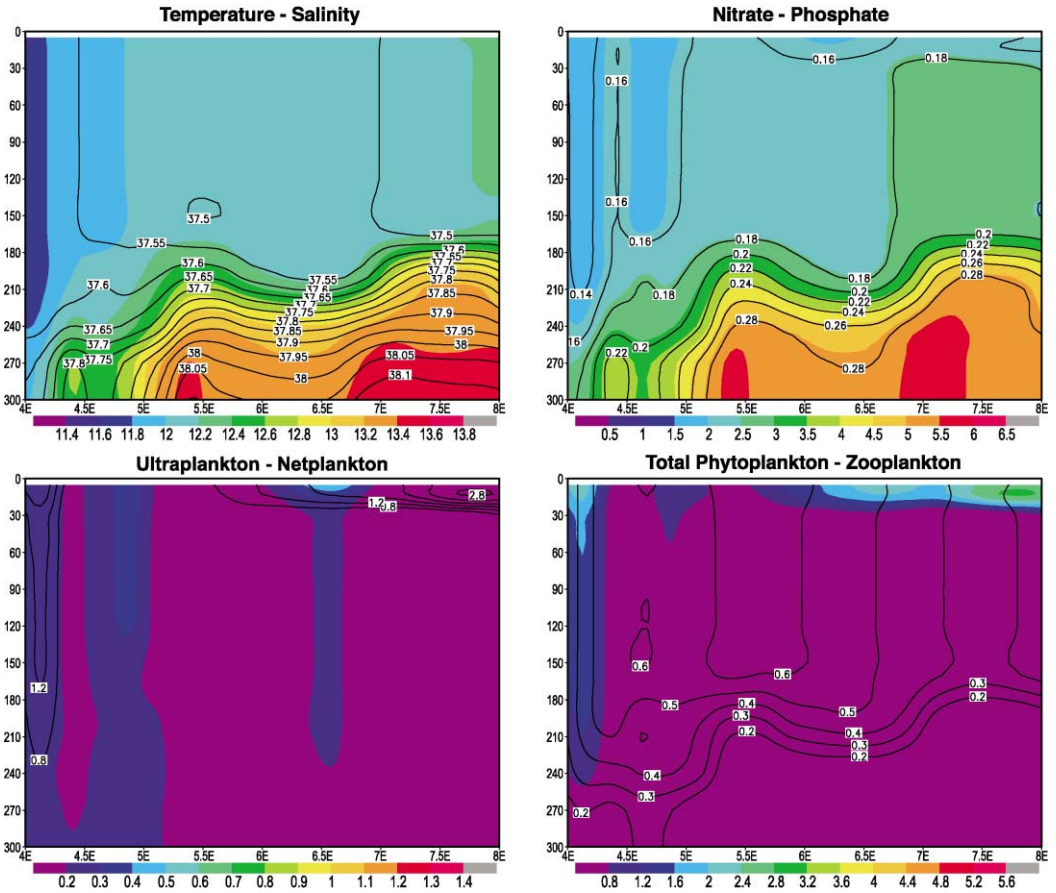

Fig. 10. Transect in Northwestern Mediterranean Sea, 42.5N 4–8E from surface to 300 m in March. From upper to bottom plates: temperature, shaded in °C, and salinity, contoured in ppt; nitrate, shaded in μM N l^{-1}, and phosphate, contoured in μM P l^{-1}; ultraplankton, shaded in μM C l^{-1}, and netplankton, contoured in μM C l^{-1}; total phytoplankton, shaded in μM C l^{-1}, and zooplankton, contoured in μM C l^{-1}.

is now confined to the first 80 m, with values from 0.4 to 1.4 μM C l^{-1}.

A comparison between Fig. 10 and Fig. 11 confirms that the onset of the vernal bloom is fueled by nutrient availability in the upper layer, but the necessary condition is the stratification of the water column.

These results can be compared with the data acquired in April 1969 during MEDIPROD I cruise. The nitrate concentrations in these data are less than 2 μM N l^{-1} in the first 50-m layer, while phosphates are less than 0.1 μM P l^{-1} in the same layer (Coste et al., 1972; Fig. 22e–f). The model's nitrate and phosphate distributions in the April stratification conditions of Fig. 11 reproduce very well these concentrations in the euphotic layer.

In the same cruise, the observed chlorophyll biomass occupies with a broad maximum the centre of the transect along the first 30-m layer (Jacques et al., 1973; Fig. 2c). The model is in agreement with this spatial location of the biomass, considering the high value position reached by the total phytoplankton concentrations of Fig. 11.

Also, zooplanktonic biomass in the first 20-m layer can be compared with the reference values from 0.15 to 0.75 μM N l^{-1} obtained by Andersen and Nival (1988) starting from 1967 to 1971 copepods abundance measures, originally expressed in dry weight. After the

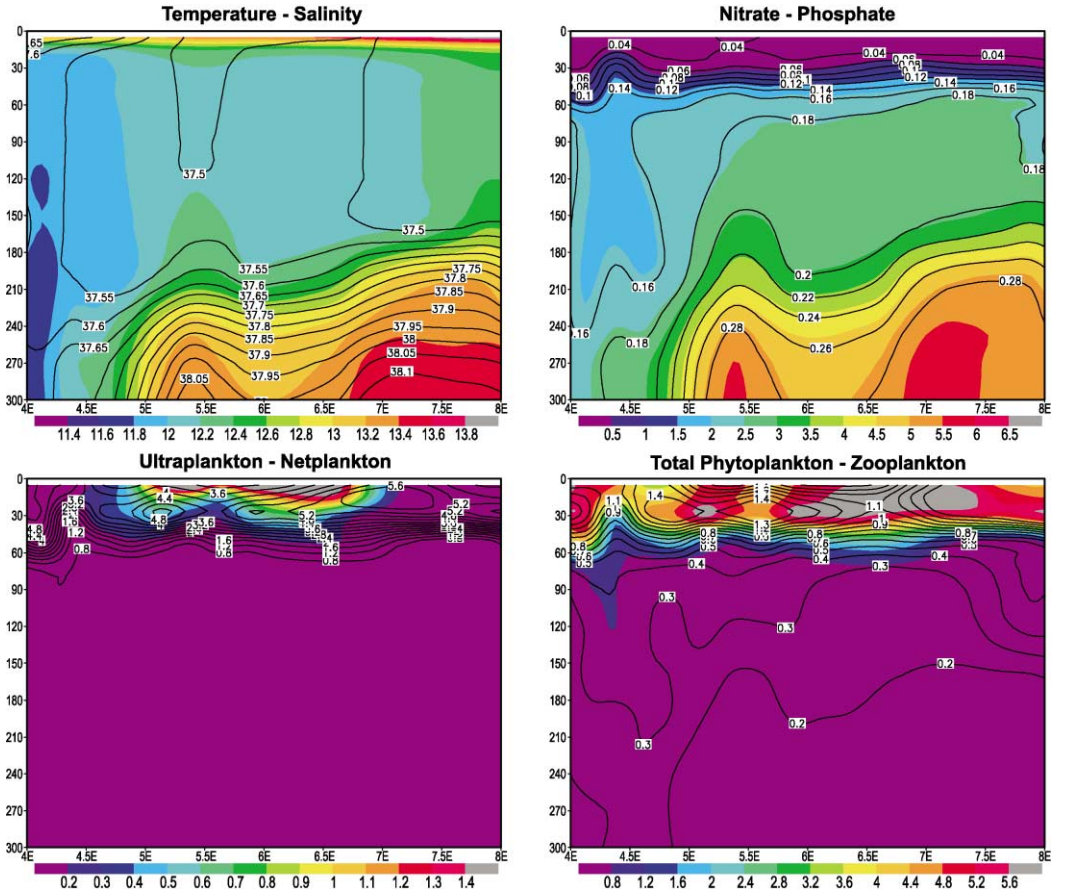

Fig. 11. Transect in Northwestern Mediterranean Sea, 42.5N 4–8E from surface to 300 m in April. From upper to bottom plates: temperature, shaded in °C, and salinity, contoured in ppt; nitrate, shaded in μM N l^{-1}, and phosphate, contoured in μM P l^{-1}; ultraplankton, shaded in μM C l^{-1}, and netplankton, contoured in μM C l^{-1}; total phytoplankton, shaded in μM C l^{-1}, and zooplankton, contoured in μM C l^{-1}.

transformation into carbon using the N:C ratio for the zooplankton, r_{NC}, a range from 0.6 to 3.0 μM C l^{-1} is obtained. The model's results are well inside this interval; in fact, the zooplanktonic biomass of Fig. 11 range from 0.9 to 1.3 μM C l^{-1}.

5.3. Ecosystem response

At a basin scale, other works, 3D (Crise et al., 1999) and box model (Crispi et al., 2001), explain the presence of the toward west increasing nutrient gradient. In the present paper, ECHYM shows how this more detailed model is used to analyse the spatial distribution for the biomass subjected to seasonal forcing.

The westerly drift of both total phytoplankton and zooplankton is evidenced in Fig. 12, where a transect at 12–20E encompassing the Sicily Strait and the Ionian Sea is shown. Meridional average is taken to mean the effects that give stronger levels in the northern part and lower ones in the southern areas.

The nutrients shoaling is clear in the upper plate with nitrates (shaded) and phosphate (contoured). This can be noted from the deepening of the 0.06 μM P l^{-1} phosphate isoline, which is at 40 m in the western area and is found at 60 m in the eastern part of the transect.

This situation produces two effects. In the lower plate, with total phytoplankton (shaded) and zooplank-

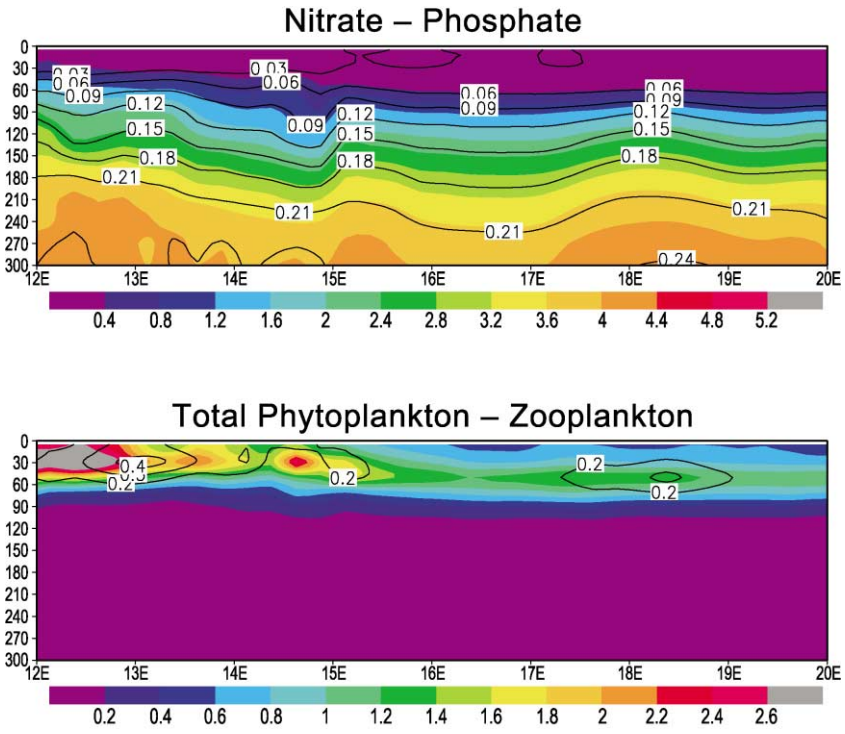

Fig. 12. Meridionally averaged transect across Sicily Strait and Ionian Sea, 12–20E from surface to 300 in October. In the upper plate nitrate, shaded in μM N l^{-1}, and phosphate, contoured in μM P l^{-1}, are shown. In the bottom plate total phytoplankton, shaded in μM C l^{-1}, and zooplankton, contoured in μM C l^{-1}, are shown.

ton (contoured), the biomass deepens from 20–30 to 50–60 m eastward bound. Moreover, the total phytoplankton maxima become consistently smaller, with higher values in the western areas and lower values in the eastern ones. Zooplankton shows a similar behaviour, with higher variabilities that, in part, obscure the overall trend.

As a qualitative comparison, the averaged values along 15–20E transect measured in 1991 during the cruise POEM-BC-O91, as reported by Rabitti et al. (1994b; Fig. 4), is considered. In particular, the phytoplankton cell abundance gives a maximum around 50 m, with a population about twice that observed at surface. This is in good agreement with the model results where the total phytoplankton has its maximum at 50–60 m with a value around 1.3 μM C l^{-1}, while the biomass decreases down to 0.5 μM C l^{-1} at surface.

Moving from the subbasin scale to global scale estimate in Table 2, the biomass divided into its ultraplankton, netplankton and zooplankton components is reported in the western basin. The integration is made along all the water column giving the minimum value, the maximum value and the average reached during the evolution. This gives the quantification of the representative values and of the excursions during seasonal variability of the three biological variables.

The averages show that netplankton is effectively favoured throughout the year and attains about two times the ultraplankton biomass. The zooplankton

Table 2
Vertically integrated biomasses in the western basin expressed in g C m^{-2}

Group	Minimum	Maximum	Average
Ultraplankton	0.5	1.8	0.9
Netplankton	1.0	3.3	1.8
Zooplankton	0.5	1.9	1.0

value is lower and reaches values of the same order as the ultraplankton ones. The excursions are about three times the minima for phytoplankters and about four times for zooplankton; moreover, there is a slight prevalence of lower values with respect to higher ones during evolution.

The maxima of total phytoplankton are in correspondence with the spring bloom and attain an average value of 5.1 g C m^{-2}. This is in good agreement with measures in the Northwestern Mediterranean (Nival et al., 1975) that give integrated averaged values from 4.6 to 5.6 g C m^{-2} along the upper 200 m during spring. The zooplankton measures, again integrated in the first 200 m, gave excursion from 0.2 g C m^{-2} in March to 1.2 g C m^{-2} in April. These values are of the same order of the zooplankton minimum and maximum reported in Table 2.

The vertically integrated biomasses are reported in Table 3 for the pelagic eastern basin, again divided into the three biological groups. The situation here is reversed with respect to Table 2; effectively higher averages are obtained for ultraplankton, about three times the netplankton ones. Their variability is lower for ultraplankton, also with prevalent lower values.

The efficient decreasing of the total phytoplankton from the western, 2.7 g C m^{-2}, to the eastern basin, 2.3 g C m^{-2}, is not so striking, as expected by CZCS estimates (see Fig. 7). The eastern phytoplankton biomass expressed in carbon units is estimated as being about 85% the average value of the western part. The figure reduce to 72% when maxima are considered.

For what concerns the zooplankton in the western basin, the average, 1.0 g C m^{-2}, is around three times the eastern basin one 0.3 g C m^{-2}. This is in line with the phytoplankton composition in the basins: in ECHYM, zooplankton, being representative of large individuals, therefore, grazes more efficiently netplankton, which is abundant in the west, than ultraplankton, dominant in the eastern basin.

Table 3
Vertically integrated biomasses in the eastern basin, Adriatic and Aegean excluded, expressed in g C m^{-2}

Group	Minimum	Maximum	Average
Ultraplankton	1.3	2.7	1.7
Netplankton	0.3	1.0	0.6
Zooplankton	0.1	0.6	0.3

Table 4
Yearly primary and secondary productions, expressed in g C m^{-2} $year^{-1}$, in the western basin and in the eastern basin, Adriatic and Aegean excluded

	Western basin	Eastern basin
Ultraplankton production	32	38
Netplankton production	88	18
Total primary production	120	56
Secondary production	13	4

Thus, the zooplankton is nearly depleted in the eastern basin and has a greater relative variability around its central value. A threefold diminution of the zooplankton average value and variability, relative to the western abundance, is emerging from data in terms of cell counts and wet weight (Kovalev et al., 1999).

Focussing on the primary and secondary productions, these annual means are reported in Table 4.

The total net primary production amount, in the western basin, to 120 g C m^{-2} $year^{-1}$, effectively more than twice that in the eastern one, without considering Adriatic and Aegean, estimated in 56 g C m^{-2} $year^{-1}$. Spatial reverse of the two fractions is made clear in this table with a dominance of netplankton production in the western basin, while in the eastern one, the ultraplankton is more productive.

The difference in the secondary production is even more striking. Herbivorous production is 13 g C m^{-2} $year^{-1}$ in the western basin, which amounts more than three times the eastern one, estimated at 4 g C m^{-2} $year^{-1}$. Generally, the herbivorous production is estimated in about 10% of the net primary production in both basins.

Data obtained during three cruises in the northwestern Mediterranean and two cruises in the Cretan Sea are reported by Turley et al. (2000). Interpreting these data as rough annual averages (months are November–April/May–July and March–September, respectively), obtained primary productions are 183 g C m^{-2} $year^{-1}$ for the western and 55 g C m^{-2} $year^{-1}$ for the eastern Mediterranean. These values indicate that northwestern Mediterranean, though intermediate between Alboran and Tyrrhenian, produces more than the average of all the western basin. On the other hand, oligotrophic Cretan Sea appears very near to the average oligotrophic conditions spread throughout the eastern basin.

Other estimates obtained by means of a light-photosynthesis 1D model (Antoine et al., 1995) give as

yearly averaged primary productions: 157.7 g C m^{-2} $year^{-1}$ for the western basin and 109.4 g C m^{-2} $year^{-1}$ for the eastern one including Adriatic and Aegean.

The summarizing comment to these higher values is the increasing role of the nutrient limitation going from west to east, inducing a diminution of about 25% in the west and 40% in the east, with respect to the 'optimal' productivities produced by the light intensity alone.

6. Conclusions

In this work, biochemistry of the Mediterranean Sea is modelled, starting from the known phenomenology of the physical forcings, of the chemical profiles and of the biological peculiarities.

A quasi-stationary evolution is obtained without using any constraints upon the biological compartments.

In fact, the buoyancy content act as a preconditioning of the trophic characteristics of the upper layer in winter time, influencing the level, but not the timing of the onset of spring bloom. Thus, the nutrient reminerализations considered in the model are able to enrich intermediate layers for the next winter supply into the euphotic zone. This is evaluated by means of the biogenic downward fluxes, which are responsible of the Mediterranean oligotrophy, and zonal trophic gradients in the decadal and longer periods.

The surface biomass is compared with the CZCS, after transforming the carbon content given by the model into chlorophyll concentrations using a statistical approach. The results of the western part in terms of averaged values behave very well in comparison with CZCS data, also with a high correlation; in the eastern part also, there is a good resemblance, with a significant correlation between model and data.

The model's results for the biomasses are obtained after dividing the overall Mediterranean into western and eastern basins. The reverse of the dominance between the two phytoplanktonic groups is nearly symmetrical with a higher presence of netplankton in the western basin and dominance of ultraplankton in the eastern one. The situation of zooplankton depletion is striking in the east, while zooplankton level is approximately threefold in the west, reaching at least the levels of ultraplankton concentrations.

The productions follow strictly the trophic gradient of the two basins. Secondary production attains 10% of the total primary production.

Acknowledgements

This work was supported by the European Commission project MAss Transfer and Ecosystem Response, no. MAS3-CT96-0051. The authors wish to thank Vittorio Barale at the Mediterranean Environment Unit of the European Community Joint Research Centre for information about CZCS data processing. We thank the Consorzio Interuniversitario del Nord–Est Italiano per il Calcolo Automatico and our colleague Valentina Mosetti for assisting us with the computer facilities.

Appendix A

The sources and sinks at each grid point for phosphate, nitrate, ammonia and dissolved oxygen, respectively, P, N, A, O, follow; all expressed in $\mu M\ l^{-1}$:

$$\begin{aligned}\mathrm{grid}_P &= R_{\mathrm{PC}}k^*_{\mathrm{rS}}S + R_{\mathrm{PC}}k^*_{\mathrm{rL}}L + R_{\mathrm{PC}}k^*_{\mathrm{eS}}S \\ &\quad + R_{\mathrm{PC}}k^*_{\mathrm{eL}}L + r_{\mathrm{PC}}k^*_{\mathrm{exz}}Z + k^*_{\mathrm{dec}P}D_{\mathrm{P}} \\ &\quad - R_{\mathrm{PC}}\mu_S f(I) g_S(T)\frac{P}{P+k_{\mathrm{PS}}} \\ &\quad \times \left[\frac{N}{N+k_{\mathrm{NS}}}\mathrm{e}^{-\psi_S A} + \frac{A}{A+k_{\mathrm{AS}}}\right]S \\ &\quad - R_{\mathrm{PC}}\mu_L f(I) g_L(T)\frac{P}{P+k_{\mathrm{PL}}} \\ &\quad \times \left[\frac{N}{N+k_{\mathrm{NL}}}\mathrm{e}^{-\psi_L A} + \frac{A}{A+k_{\mathrm{AL}}}\right]L, \end{aligned} \tag{1}$$

$$\begin{aligned}\mathrm{grid}_N &= k^*_{\mathrm{nit}}\frac{O}{O+k_{\mathrm{AO}}}A - R_{\mathrm{NC}}\mu_S f(I) g_S(T) \\ &\quad \times \frac{P}{P+k_{\mathrm{PS}}}\frac{N}{N+k_{\mathrm{NS}}}\mathrm{e}^{-\psi_S A}S \\ &\quad - R_{\mathrm{NC}}\mu_L f(I) g_L(T)\frac{P}{P+k_{\mathrm{PL}}} \\ &\quad \times \frac{N}{N+k_{\mathrm{NL}}}\mathrm{e}^{-\psi_L A}L, \end{aligned} \tag{2}$$

$$\begin{aligned}\mathrm{grid}_A = {} & R_{\mathrm{NC}}k^*_{\mathrm{rS}}S + R_{\mathrm{NC}}k^*_{\mathrm{rL}}L + R_{\mathrm{NC}}k^*_{\mathrm{eS}}S \\ & + R_{\mathrm{NC}}k^*_{\mathrm{eL}}L + k^*_{\mathrm{decN}}D_{\mathrm{N}} + r_{\mathrm{NC}}k^*_{\mathrm{exz}}Z \\ & + R_{\mathrm{NC}}g\left(1 - \frac{R_{\mathrm{PC}}r_{\mathrm{NC}}}{R_{\mathrm{NC}}r_{\mathrm{PC}}}\right)\frac{\epsilon_S S + \epsilon_L \alpha L}{S + \alpha L + k}Z \\ & - k^*_{\mathrm{nit}}\frac{O}{O + k_{\mathrm{AO}}}A - R_{\mathrm{NC}}\mu_S f(I)g_S(T) \\ & \times \frac{P}{P + k_{\mathrm{PS}}}\frac{A}{A + k_{\mathrm{AS}}}S \\ & - R_{\mathrm{NC}}\mu_L f(I)g_L(T)\frac{P}{P + k_{\mathrm{PL}}}\frac{A}{A + k_{\mathrm{AL}}}L, \end{aligned} \quad (3)$$

$$\begin{aligned}\mathrm{grid}_O = {} & R_{\mathrm{OC}}\mu_S f(I)g_S(T)\frac{P}{P + k_{\mathrm{PS}}} \\ & \times \left[\frac{N}{N + k_{\mathrm{NS}}}\mathrm{e}^{-\psi_S A} + \frac{A}{A + k_{\mathrm{AS}}}\right]S \\ & + R_{\mathrm{OC}}\mu_L f(I)g_L(T)\frac{P}{P + k_{\mathrm{PL}}} \\ & \times \left[\frac{N}{N + k_{\mathrm{NL}}}\mathrm{e}^{-\psi_L A} + \frac{A}{A + k_{\mathrm{AL}}}\right]L - R_{\mathrm{OC}}k^*_{\mathrm{rS}}S \\ & - R_{\mathrm{OC}}k^*_{\mathrm{rL}}L - R_{\mathrm{nit}}k^*_{\mathrm{nit}}\frac{O}{O + k_{\mathrm{AO}}}A \\ & - R_{\mathrm{OC}}k^*_{\mathrm{decC}}D_{\mathrm{C}} + \mathrm{rel}_O. \end{aligned} \quad (4)$$

The expressions for S and L, respectively, concentrations of ultraplankton and netplankton expressed in μM C l^{-1}, and for Z, zooplankton variable in the same unit, can be found below:

$$\begin{aligned}\mathrm{grid}_S = {} & \mu_S f(I)g_S(T)\frac{P}{P + k_{\mathrm{PS}}} \\ & \times \left[\frac{N}{N + k_{\mathrm{NS}}}\mathrm{e}^{-\psi_S A} + \frac{A}{A + k_{\mathrm{AS}}}\right]S - d_S S \\ & - k^*_{\mathrm{rS}}S - k^*_{\mathrm{eS}}S - \frac{SZ}{\alpha L + S + k_{\mathrm{H}}}, \end{aligned} \quad (5)$$

$$\begin{aligned}\mathrm{grid}_L = {} & \mu_L f(I)g_L(T)\frac{P}{P + k_{\mathrm{PL}}} \\ & \times \left[\frac{N}{N + k_{\mathrm{NL}}}\mathrm{e}^{-\psi_L A} + \frac{A}{A + k_{\mathrm{AL}}}\right]L - d_L L \\ & - k^*_{\mathrm{rL}}L - k^*_{\mathrm{eL}}L - \frac{\alpha LZ}{\alpha L + S + k_{\mathrm{H}}}, \end{aligned} \quad (6)$$

$$\mathrm{grid}_Z = g\frac{R_{\mathrm{PC}}}{r_{\mathrm{PC}}}\frac{\epsilon_S S + \epsilon_L \alpha L}{S + \alpha L + k_{\mathrm{H}}}Z - d_Z Z - k^*_{\mathrm{exz}}Z. \quad (7)$$

The three equations for detritus, expressed in μM l^{-1}, follow, in carbon units, D_{C}, in nitrogen units, D_{N}, and in phosphorus units, D_{P}, respectively:

$$\begin{aligned}\mathrm{grid}_{D_{\mathrm{C}}} = {} & d_Z Z + d_S S + d_L L + (1 - \epsilon_S) \\ & \times \frac{gSZ}{S + \alpha L + k_{\mathrm{H}}} + (1 - \epsilon_L) \\ & \times \frac{g\alpha LZ}{S + \alpha L + k_{\mathrm{H}}} - k^*_{\mathrm{decC}}D_{\mathrm{C}}, \end{aligned} \quad (8)$$

$$\begin{aligned}\mathrm{grid}_{D_{\mathrm{N}}} = {} & r_{\mathrm{NC}}d_Z Z + R_{\mathrm{NC}}d_S S + R_{\mathrm{NC}}d_L L + R_{\mathrm{NC}} \\ & \times \left\{(1 - \epsilon_S)\frac{gSZ}{S + \alpha L + k_{\mathrm{H}}}\right. \\ & \left. + (1 - \epsilon_L)\frac{g\alpha LZ}{S + \alpha L + k_{\mathrm{H}}}\right\} - k^*_{\mathrm{decN}}D_{\mathrm{N}}, \end{aligned} \quad (9)$$

$$\begin{aligned}\mathrm{grid}_{D_{\mathrm{P}}} = {} & r_{\mathrm{PC}}d_Z Z + R_{\mathrm{PC}}d_S S + R_{\mathrm{PC}}d_L L + R_{\mathrm{PC}} \\ & \times \left\{(1 - \epsilon_S)\frac{gSZ}{S + \alpha L + k_{\mathrm{H}}}\right. \\ & \left. + (1 - \epsilon_L)\frac{g\alpha LZ}{S + \alpha L + k_{\mathrm{H}}}\right\} - k^*_{\mathrm{decP}}D_{\mathrm{P}}. \end{aligned} \quad (10)$$

All parameters with an asterisk represent multiplication of the parameter itself with the temperature-dependent factor, θ^{T-T_0}. The nutrient limitations for the phytoplankton growths, flim_S and flim_L, are expressed in terms of phosphate, nitrate and ammonia:

$$\mathrm{flim}_S = \frac{P}{P + k_{\mathrm{PS}}}\left[\frac{N}{N + k_{\mathrm{NS}}}\mathrm{e}^{-\psi_S A} + \frac{A}{A + k_{\mathrm{AS}}}\right], \quad (11)$$

$$\mathrm{flim}_L = \frac{P}{P + k_{\mathrm{PL}}}\left[\frac{N}{N + k_{\mathrm{NL}}}\mathrm{e}^{-\psi_L A} + \frac{A}{A + k_{\mathrm{AL}}}\right]. \quad (12)$$

The light limitation, $f(I)$, is given by:

$$f(I) = \mathrm{rf}\frac{I\mathrm{e}^{-k_z z}}{I_{\mathrm{opt}}}\mathrm{e}^{1 - \frac{I\mathrm{e}^{-k_z z}}{I_{\mathrm{opt}}}}. \quad (13)$$

Here, I is the incident radiation at the sea surface:

$$I = I_0(1 - 0.62\mathrm{cl} + 0.0019\mathrm{sb}), \quad (14)$$

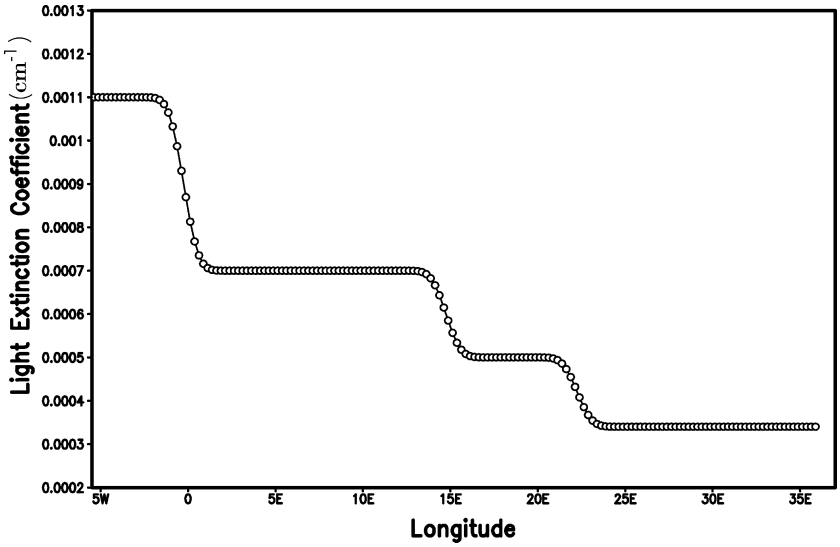

Fig. 13. Model's light extinction coefficient, k_z, cm^{-1}, vs. longitude.

where I_0 is the total radiation reaching sea surface in absence of cloud coverage, cl, and sb is the solar noon altitude in degrees. The normalized daylength, rf, is:

$$\mathrm{rf} = \arccos(-\tau(\mathrm{dc}))\tau(\phi)/\pi \tag{15}$$

function of the sun declination, dc.

The zonally variant, k_z, is given in Fig. 13, as obtained from Secchi disk data measured by the POEM Group (Rabitti et al., 1994a,b) for the Eastern Mediterranean, and during the EROS 2000 project (Martin and Barth, 1995) for the Western Mediterranean.

The limitations due to the temperature, T, are:

$$g_S(T) = \left(\frac{T_{S_{\max}} - T}{T_{S_{\max}} - T_S}\right)^{b_S(T_{S_{\max}} - T_S)} \mathrm{e}^{b_S(T - T_S)}, \tag{16}$$

$$g_L(T) = \left(\frac{T_{L_{\max}} - T}{T_{L_{\max}} - T_L}\right)^{b_L(T_{L_{\max}} - T_L)} \mathrm{e}^{b_L(T - T_L)}. \tag{17}$$

The only biochemical constraint of the ecosystem is oxygen relaxation performed at the surface level using by the reaeration process:

$$rel_O = k_{\mathrm{aer}}(O_{\mathrm{sat}} - O), \tag{18}$$

where O_{sat} is the oxygen saturation function of the temperature and the salinity, as in Gromiec (1983):

$$O_{\mathrm{sat}} = 457.01 - 11.47T + 0.14T^2 - 3.02S + 0.064TS + 0.0086S^2. \tag{19}$$

Finally, the statistical model by Cloern et al. (1995) is used to transform the carbon content of the net-plankton into chlorophyll concentrations through the following expression:

$$C_L = (0.003 + 0.0154\mathrm{e}^{0.050T}\mathrm{e}^{-0.059(I_0/k_z z_0(1-\mathrm{e}^{-k_z z_0})}\mathrm{flim}_L)L, \tag{20}$$

and analogously the ultraplankton carbon content is transformed using:

$$C_S = (0.003 + 0.0154\mathrm{e}^{0.050T}\mathrm{e}^{-0.059(I_0/k_z z_0(1-\mathrm{e}^{-k_z z_0})}\mathrm{flim}_S)R_{SL}S, \tag{21}$$

where C_S and C_L are the chlorophyll concentrations (mg Chl m^{-3}) in the ultraplankton and in the net-plankton compartment, respectively; T is the temperature (°C), I_0 is the irradiance at the surface (mol quanta m^{-2} day^{-1}); z_0 is the upper layer depth; and

R_{SL} is the transformation quota of the chlorophyll to carbon coefficient from netplankton to ultraplankton in specific conditions. Thus, the chlorophyll is diagnostically calculated assuming the irradiance, the temperature and the nutrients availability as parameterized in the model. Such a transformation is performed on biomasses and nutrients averaged in the 20-m upper layer.

References

Andersen, V., Nival, P., 1988. Modèle d' écosystème pélagique des eaux côtières de la Mer Ligure. Oceanol. Acta 9 (SP), 211–217.

Antoine, D., Morel, A., André, J.-M., 1995. Algal pigment distribution and primary production in the eastern Mediterranean as derived from coatal zone color scanner observations. J. Geophys. Res. 100 (C8), 16, 193-16, 209.

Azam, F., Fenchel, T., Field, J.G., Gray, J.S., Meyer-Reil, L.A., Thingstad, T.F., 1983. The ecological role of water-column microbes in the sea. Mar. Ecol. Prog. Ser. 10, 257–263.

Barale, V., Larkin, D., Fusco, L., Melinotte, J.M., Pittella, G., 1999. OCEAN Project: the European archive of CZCS historical data. Int. J. Remote Sens. 20 (7), 1201–1218.

Beers, J.R., 1966. Studies on the chemical composition of the major zooplankton groups in the Sargasso Sea off Bermuda. Limnol. Oceanogr. 11, 520–528.

Berland, B., Bonin, D., Coste, B., Maestrini, S., Minas, H.J., 1973. Influence des conditiones hivernales sur les productions phyto- et zooplanctoniques en Méditerranée Nord-Occidentale: III. Caractérisation des eaux de surface au moyen de cultures d'algues. Mar. Biol. 23, 267–274.

Berman, T., Townsend, D.W., El Sayed, S.Z., Trees, C.C., Azov, Y., 1984. Optical transparency, chlorophyll and primary productivity in the Eastern Mediterranean near Israeli coast. Oceanol. Acta 7 (3), 367–372.

Béthoux, J.B., Morin, P., Madec, C., Gentili, B., 1992. Phosphorus and nitrogen behaviour in the Mediterranean Sea. Deep-Sea Res. 39 (9), 1641–1654.

Bisset, W.P, Meyers, M.B., Walsh, J.J, Müller-Karger, F.E., 1994. The effects of temporal variability of mixed layer depth on primary productivity around Bermuda. J. Geophys. Res. 99 (C4), 7539–7553.

Brand, L.E., Guillard, R.R.L., 1981. The effects of continuous light and light intensity on the reproduction rates of twenty-two species of marine phytoplankton. J. Exp. Mar. Biol. Ecol. 50, 119–132.

Castellari, S., Pinardi, N., Leaman, K., 1998. A model study of air–sea interactions in the Mediterranean Sea. J. Mar. Syst. 18 (1–3), 89–114.

Civitarese, G., Crise, A., Crispi, G., Mosetti, R., 1996. Circulation effects on nitrogen dynamics in the Ionian Sea. Oceanol. Acta 19 (6), 609–622.

Civitarese, G., Gacic, M., Vetrano, A., Boldrin, A., Bregant, D., Rabitti, S., Souvermezoglou, E., 1998. Biochemical fluxes through the Strait of Otranto (Eastern Mediterranean). Cont. Shelf Res. 18, 773–789.

Cloern, J.E., Grenz, C., Vidergas-Lucas, L., 1995. An empirical model of the phytoplankton chlorophyll:carbon ratio—the conversion factor between productivity and growth rate. Limnol. Oceanogr. 40 (7), 1313–1321.

Coste, B., Gostan, J., Minas, H.J., 1972. Influence des conditions hivernales sur les productions Phyto-et Zooplanctoniques en Méditerranée Nord-Occidentale: I. Structures Hydrologiques et Distributions des Sels Nutritifs. Mar. Biol. 23, 251–265.

Coste, B., Le Corre, P., Minas, H.J., 1988. Re-evaluation of the nutrient exchanges in the Strait of Gibraltar. Deep-Sea Res. 35, 767–775.

Crise, A., Crispi, G., Mauri, E., 1998. A seasonal three-dimensional study of the nitrogen cycle in the Mediterranean Sea: Part I. Model implementation and numerical results. J. Mar. Syst. 18 (1–3), 287–312.

Crise, A., Allen, J.I., Baretta, J., Crispi, G., Mosetti, R., Solidoro, C., 1999. The Mediterranean pelagic ecosystem response to physical forcing. Prog. Oceanogr. 44, 219–243.

Crispi, G., Crise, A., Mauri, E., 1999. A seasonal three-dimensional study of the nitrogen cycle in the Mediterranean Sea: Part II. Verification of the energy constrained trophic model. J. Mar. Syst. 20 (1–4), 357–379.

Crispi, G., Mosetti, R., Solidoro, C., Crise, A., 2001. Nutrients cycling in Mediterranean basins: the role of the biological pump in the trophic regime. Ecol. Model. 138 (1–3), 101–114.

Davis, C.S., 1987. Components of the zooplankton production cycle in the temperate ocean. J. Mar. Res. 45, 947–983.

Denis-Karafistan, A., Martin, J.-M., Minas, H., Brasseur, P., Nihoul, J., Denis, C., 1998. Space and seasonal distributions of nitrates in the Mediterranean Sea derived from a variational inverse model. Deep-Sea Res. 45, 387–408.

Dugdale, R.C., Wilkerson, F.P., 1988. Nutrient sources and primary production in the Eastern Mediterranean. Oceanol. Acta 9, 179–184.

Eppley, R.W., Peterson, B.J., 1979. Particulate organic matter flux and planktonic new production in the deep ocean. Nature 282, 677–680.

Eppley, R.W., Sharp, J.H., Renger, E.H., Perry, M.J., Harrison, W.G., 1977. Nitrogen assimilation by phytoplankton and other microorganisms in the surface waters of the North Pacific Ocean. Mar. Biol. 39, 111–120.

Fasham, M.J.R., Duklow, H.W., McKelvie, S.M., 1990. A nitrogen-based model of plankton dynamics in the oceanic mixed layer. J. Mar. Res. 48, 591–639.

Fiala, M., Kopczynska, E.E., Jeandel, C., Oriol, L., Vetion, G., 1998. Seasonal and interannual variability of size-fractionated phytoplankton biomass and community structure at station Kerfix of the Kerguelen Islands, Antarctica. J. Plankton Res. 20 (7), 1341–1356.

Glover, H.E., Prezelin, B.P., Campell, L., Wyman, M., Garside, C., 1988. A nitrate-dependent *Synechococcus* bloom in surface Sargasso Sea water. Nature 331, 161–163.

Gromiec, M.J., 1983. Biochemical Demand—Dissolved Oxygen. Application of Ecological Modelling in Environmental Management, Part A. Elsevier, Amsterdam.

Holling, C.S., 1965. The functional response of predators to prey density. Mem. Entomol. Soc. Can. 45, 5–60.

Jacques, G., Minas, H.J., Minas, M., Nival, P., 1973. Influence des conditions hivernales sur les productions phyto- et zooplanctoniques en Méditerranée Nord-Occidentale: II. Biomasse et production phytoplanctonique. Mar. Biol. 23, 251–265.

Kana, T.M., Glibert, P.M., 1987. Effect of irradiances up to 2000 $\mu Em^{-2} s^{-1}$ on marine *Synechococcus* WH7803: I. Growth, pigmentation, and cell composition. Deep-Sea Res. 34 (4), 479–495.

Kovalev, A.V., Kideys, A.E., Pavlova, E.V., Shmeleva, A.A., Skryabin, V.A., Ostrovskaya, N.A., Uysal, Z., 1999. Composition and abundance of zooplankton of the Eastern Mediterranean Sea. In: Malanotte-Rizzoli, P., Eremeev, V.N. (Eds.), The Eastern Mediterranean as a Laboratory Basin for the Assessment of Contrasting Ecosystems, Kluwer Scientific Publishing, Dordrecht, pp. 81–95.

Krom, M.D., Brenner, S., Kress, N., Neori, A., Gordon, L.I., 1993. Nutrient distribution during an annual cycle across a warm-core eddy from the E. Mediterranean Sea. Deep-Sea Res. 40 (4), 805–825.

Lassiter, R.R., Kearns, D.K., 1974. Phytoplankton population changes and nutrient fluctuations in a simple aquatic ecosystem model. In: Middlebrookes, E.J., Falkenberg, D.H., Maloney, T.E. (Eds.), Modeling the Eutrophication Process, Ann Arbor Sci. Publ., Ann Arbor, MI, pp. 131–138.

Lefevre, D., Minas, H.J., Minas, M., Robinson, C., Williams, P.J., Le, B., Woodward, E.M.S., 1997. Review of gross community production, primary production, net community production and dark community respiration in the Gulf of Lions. Deep-Sea Res., Part II 44 (3–4), 801–832.

Levitus, S., Conkright, M.E., Reid, J.L., Najjar, R., Mantyla, A., 1993. Distribution of nitrate, phosphate and silicate in the world ocean. Prog. Oceanogr. 31, 245–273.

Levy, M., Memery, L., Madec, G., 1999. The onset of the Spring Bloom in the MEDOC area: mesoscale spatial variability. Deep-Sea Res. 46, 1137–1160.

Llewellyn, C.A., Gibb, S.W., 2000. Intra-class variability in the carbon, pigment and biomineral content of prymnesiophytes and diatoms. Mar. Ecol. Prog. Ser. 193, 33–44.

Marcer, R., Fraunie, P., Dekeyser, I., Andersen, V., 1991. Numerical modelling of biological–physical interactions in coastal sites. Oceanol. Acta, Spec. Issue 11, 71–79.

Margalef, R., 1985. Environmental control of the mesoscale distribution of primary producers and its bearing to primary production in the Western Mediterranean. In: Moraitou-Apostolopoulou, M., Kiortsis, V. (Eds.), Mediterranean Marine Ecosystems, Plenum, New York, pp. 213–229.

Martin, J.-M., Barth, H. (Eds.), 1995. EROS 2000 (European River Ocean System) Fifth Workshop on the North–West Mediterranean Sea Hamburg (Germany), 28–30 March 1994. Water Pollution Research Report 32, EUR 16130 EN, p. 318.

McGill, D.A., 1970. Mediterranean Sea Atlas—distribution of nutrient chemical properties Woods Hole Oceanographic Institution, Woodshole, MA.

McLaren, I.A., 1965. Some relationships between temperature and egg size, body size, development rate and fecundity of the copepod *Pseudocalanus*. Limnol. Oceanogr. 10, 528–538.

Michaels, A.F., Silver, M.W., 1988. Primary production, sinking fluxes and the microbial food web. Deep-Sea Res. 35 (4), 473–490.

Nival, P., Nival, S., Thiriot, A., 1975. Influence des conditions hivernales sur les productions phyto- et zooplanctoniques en Méditerranée Nord-Occidentale: V. Biomasse et production zooplanctonique - relations phyto-zooplancton. Mar. Biol. 31, 249–270.

Pinazo, C., Marsaleix, P., Millet, B., Estournel, C., Véhil, R., 1996. Spatial and temporal variability of phytoplankton biomass in upwelling areas of the northwestern Mediterranean: a coupled physical and biogeochemical modelling approach. J. Mar. Syst. 7 (2–4), 161–191.

POEM Group, 1992. General circulation of the Eastern Mediterranean. Earth-Sci. Rev. 32, 285–309.

Rabitti, S., Civitarese, G., Ribera, M., 1994a. Data Report Cruise POEM-BC—October 1991—Ionian Basin and Sicily Channel: II. Chemical and Biologial Data. Tech. Report No. 13/94-CNR/IBM.

Rabitti, S., Bianchi, F., Boldrin, A., Daros, L., Socal, G., Totti, C., 1994. Particulate matter and phytoplankton in the Ionian Sea. Oceanol. Acta 17 (3), 297–307.

Redfield, A.C., Ketchum, B.H., Richards, F.A., 1963. The influence of Sea Water. In: Hill, M.N. (Ed.), The Sea, vol. 2. Interscience, New York, pp. 26–77.

Sakshaug, E., Andresen, K., Kiefer, D.A., 1989. A steady state description of growth and light absorption in the marine planktonic diatom *Skeletonema costatum*. Limnol. Oceanogr. 34 (1), 198–205.

Shiomoto, A., Tadokoro, K., Monaka, K., Nanba, M., 1997. Productivity of picoplankton compared with that of larger phytoplankton in the subarctic region. J. Plankton Res. 19 (7), 907–916.

Steele, J.H., 1998. Incorporating the microbial loop in a simple plankton model. Proc. R. Soc. London, Ser. B 265, 1771–1777.

Sturm, B., Barale, V., Larkin, D., Andersen, J.H., Turner, M., 1999. OCEANcode: the complete set of algorithms and models for the level-2 processing of European CZCS historical data. Int. J. Remote Sens. 20 (7), 1219–1248.

Thingstad, T.F., Rassoulzadegan, F., 1995. Nutrient limitations, microbial food webs, and 'biological C-pumps': suggested interactions in a P-limited Mediterranean. Mar. Ecol. Prog. Ser. 117, 299–306.

Turley, C.M., Bianchi, M., Christaki, U., Conan, P., Harris, J.R.W., Psarra, S., Ruddy, G., Stutt, E.D., Tselepides, A., Van Wambecke, F., 2000. Mar. Ecol. Prog. Ser. 193, 11–18.

Tusseau-Vuillemin, M.-H., Mortier, L., Herbaut, C., 1998. Modeling nitrate fluxes in an open coastal environment (Gulf of Lions): transport versus biogeochemical processes. J. Geophys. Res. 103 (C4), 7693–7708.

Wen, Y.H., Peters, R.H., 1994. Empirical models of phosphorus and nitrogen excretion rates by zooplankton. Limnol. Oceanogr. 39 (7), 1669–1679.

Wrobleski, J.S., 1977. A model of phytoplankton plume formation during variable Oregon upwelling. J. Mar. Res. 35 (2), 357–394.

Zakardjian, B., Prieur, L., 1994. A numerical study of primary production related to vertical turbulent diffusion with special reference to vertical motions of the phytoplankton cells in nutrient and light fields. J. Mar. Syst. 5, 267–295.

Zavatarelli, M., Baretta, J.W., Baretta-Bekker, J.G., Pinardi, N., 2000. The dynamics of the Adriatic Sea ecosystem: an idealized model study. Deep-Sea Res. 47, 937–970.

Zonneveld, C., 1998. A cell-based model for the chlorophyll a to carbon ratio in phytoplankton. Ecol. Model. 113, 55–70.